(NASA-CR-163919) EFFECT OF LOAD INTRODUCTION ON GRAPHITE EPOXY COMPRESSION SPECIMENS Final Report (Howard Univ.) 103 p HC A06/MF A01 CSCL 11D

N81-16138

Unclas
G3/24 41320

FINAL REPORT

NASA GRANT NAG1-23

EFFECT OF LOAD INTRODUCTION ON GRAPHITE EPOXY COMPRESSION SPECIMENS

by

Robert Reiss
Associate Professor of Mechanical Engineering
Principal Investigator

and

Tse-Min Yao
Graduate Research Assistant

HOWARD UNIVERSITY

SCHOOL OF ENGINEEREING

DEPARTMENT OF MECHANICAL ENGINEERING

WASHINGTON, D.C. 20059

January 1981

HOWARD UNIVERSITY

SCHOOL OF ENGINEERING

DEPARTMENT OF MECHANICAL ENGINEERING

WASHINGTON, D.C. 20059

FINAL REPORT

NASA GRANT NAG1-23

EFFECT OF LOAD INTRODUCTION ON GRAPHITE EPOXY COMPRESSION SPECIMENS

by

Robert Reiss
Associate Professor of Mechanical Engineering
Principal Investigator

and

Tse-Min Yao
Graduate Research Assistant

January, 1981

ABSTRACT

Compression testing of modern composite materials is affected by the manner in which the compressive load is introduced. Two such effects are investigated in this report: (a) the constrained edge effect which prevents transverse expansion and is common to all compression testing in which the specimen is gripped in the fixture; and (b) non-uniform gripping which induces bending into the specimen. This study has developed an analytical model capable of quantifying these foregoing effects. The model is based upon the principle of minimum complementary energy. For pure compression, the stresses are approximated by Fourier series. For pure bending, the stresses are approximated by Legendre polynomials.

TABLE OF CONTENTS

NOMENCLATURE

α, β	Eigenvalues
$\underline{\eta}$, $\underline{\zeta}$	Eigenvectors
ε_x, ε_y or ε_1, ε_2	Strain in the x,y or 1,2 directions
γ_{xy} or γ_{12}	Shear strain in the x-y or 1-2 plane
σ_x, σ_y or σ_1, σ_2	Stress in the x,y or 1,2 directions
$\bar{\sigma}_x$, $\bar{\sigma}_y$	Stress averaged across laminate thickness
τ_{xy}, τ_{12}	Shear stress in the x-y or 1-2 plane
$\bar{\tau}_{xy}$, $\bar{\tau}_{12}$	Averaged shear stress
Γ_o	Introduced material constant ($\Gamma_o = E_y/G_{xy} - 2\nu_{xy} \cdot E_y/E_x$)
ν	Poisson's ratio
ν_{xy}, ν_{yx}, ν_{12}, ν_{21}	Poisson's ratio in the x-y, 1-2 plane and their ccunterparts
θ	Angle between principal material coordinates and arbitrary body coordinates
ϑ°	Ridgid body rotation
∂	Partial differential
Φ	Complementary Energy Functional
ξ	Geometric ratio (Length/Width)

det	Determinant
E	Young's modulus
E_x, E_y or E_1, E_2	Young's modulus in the x, y or 1, 2 directions
G	Shear modulus
G_{xy}, G_{12}	Shear modulus in the x-y or 1-2 plane and their counterparts
$\underset{\sim}{M}$, $\underset{\sim}{C}$, $\underset{\sim}{K}$ or [M], [C], [K]	Matrices
Q-I	Quasi-isotropic
C-P	Cross-ply
U-D	Unidirectional
u^o	Rigid axial displacement

Chapter I

INTRODUCTION

A. Rationale

In compression testing, it is difficult to determine purely compressive mechanical properties of fiber-reinforced matrix laminates. Some of the experimental data showed that mechanical properties of the specimen depend strongly upon the compression fixture utilized [1]. Therefore, it is not surprising that some controversy has developed regarding acceptable techniques for compression testing.

Other than manufacturing non-uniformities in test specimens, compression data may be suspect due to uneven gripping of the tabs, poor alignment of the test machine and/or poor alignment of the test fixture. Fracture or ultimate compressive stress may be difficult to obtain because another mode of failure (i.e. buckling, delamination) may occur first.

Many of the foregoing difficulties can be lessened by selecting a short gage length specimen. At the extremities of the test specimen, the clamping mechanism of the test fixture creates a complicated stress state by preventing transverse expansion. For sufficiently short gage lengths this constrained edge effect will be evident throughout the entire specimen. A size change of the specimen, therefore, may merely substitute one difficulty for another.

The constrained edge effect has been pointed out in Refs. [2-4]. However, only the present work provides a model capable of quantifying it. This is done through stress analysis by assuming perfect alignment and two different gripping mechanisms of the fixture: (a) uniform gripping (axial compression) and (b) small in-plane bending superimposed upon axial compression.

B. Background

Pagano and Halpin [2] investigated the influence of the end constraint, both experimentally and analytically, in tension tests of anisotropic bodies, including on off-angle graphite/epoxy laminate. Their analysis was based upon the two-dimensional elastic compatibility equations. They concluded that the gripping mechanism and the length to width ratio of the specimen were the principal reasons for the non-existence of a uniform stress state. They also predicted a more serious influence of gripping in compression and torsion testing of anisotropic bodies. However, they did not quantify the end constraint. A photoelastic study of axially compressed rectangular sections, by Phillips and Mantei [3], gave some evidence of the effect of load introduction upon homogeneous, isotropic materials.

An investigation of the effect of an end attachment on the strength of fiber-reinforced axisymmetric composite cylinders was presented by Whitney, Grimes and Francis [4]. They pointed out that an end attachment which allows some deformation of the end (e.g. adhesive bond) will help alleviate the problem of high stress and strain concentration at the attachment end.

Another method of studying the edge effect in two dimensional stress analysis is based upon the Airy function. Unfortunately, the mixed form of the boundary conditions precludes any possibility of an exact solution. Hess [5] uses separable forms of the Airy function (which decay exponentially from the fixed end) to determine approximate solutions.

A related problem, whose solution also illustrates the St. Venant Principle, and has received more attention in recent years, is the free edge effect. At the traction-free edge of a compression specimen, the mismatch in the material properties at laminate interface causes a highly localized effect.

An example of the free edge effect for a biaxial stress state using methods developed in the present study would seem an interesting challenge.

The difficulty in estimating stresses in the area near the free edge, using the finite difference method presented by Pipes and Pagano [6] was pointed out by Wang and Dickson [9]. The finite element procedure developed by Wang and Crossman [7] has the same difficulties as the finite difference method. Both methods need certain artificial manipulations, specifically in the region very close to the free edge. The perturbation technique applied by Hsu and Herakovich [8] provided smooth continuous stress distributions in the vicinity of the free edge and mathematical evidence of singular interlaminar shear stresses for cross-ply graphite/epoxy laminates. Another method of estimating the interlaminar shear stresses is based upon the Galerkin method [9].

In the subsequent chapters, an analytical method is presented for quantifying the constrained edge effect.

C. Specific Objectives

The objectives of this study are:

1. To develop a closed form approximation to the stress distribution within each lamina of high-strength graphite/epoxy during compression tests.
2. To determine the effect of specimen geometry upon the measured compressive properties, including the determination of the minimum specimen gage length necessary for the existence of a uniform compressive state in the central region of the specimen.
3. To determine the effect of small in-plane bending upon the measured compressive properties.
4. To determine the optimal location of strain gages for compression tests.

Chapter II

PROBLEM FORMULATION

A. Statement of the Problem

The primary objective of this study is to determine the effect of testing devices on the response of compression (tensile) specimens of laminate composites which are symmetric about their middle plane. For the case of perfect alignment and perfect gripping in a rigid fixture, the ends of the specimen will undergo the rigid displacement shown in Fig. 1, where u° and θ° denote the uniform displacement and rotation of the constrained edges, respectively. Also, L and b are the respective half length and half width of the specimen, and x and y are Cartesian coordinates measured from the specimen's center.

B. Modelling Assumptions

The laminate theory for fiber layups which are symmetric about the middle plane is applied here. Thus throughout the laminate there exists a generalized plane

PRECEDING PAGE BLANK NOT FILMED

state of stress whose Cartesian components are denoted by $\bar{\sigma}_x$, $\bar{\sigma}_y$ and $\bar{\tau}$. The bars above the stress symbols indicate quantities averaged across the laminate thickness.

With the assumptions of small displacements and a linear orthotropic constitutive response, the field equations to be satisfied are:

1. equilibrium equations

$$\partial\bar{\sigma}_x/\partial x + \partial\bar{\tau}/\partial y = 0,$$

$$\partial\bar{\tau}/\partial x + \partial\bar{\sigma}_y/\partial y = 0; \qquad (1)$$

2. strain-displacement relations

$$\varepsilon_x = \partial u/\partial x,$$

$$\varepsilon_y = \partial v/\partial y,$$

$$\gamma = \partial u/\partial y + \partial v/\partial x; \qquad (2)$$

3. constitutive equations

$$\varepsilon_x = S_{11}\bar{\sigma}_x + S_{12}\bar{\sigma}_y,$$

$$\varepsilon_y = S_{12}\bar{\sigma}_x + S_{22}\bar{\sigma}_y,$$

$$\gamma = S_{44}\bar{\tau}; \qquad (3)$$

In Eqs. (2), u and v denote the displacements in the x (loading) and y (transverse in the plane of the specimen) directions, respectively. The material constants S_{ij} can be computed directly from the known material constants of the constituent laminae and their fiber orientations with respect to the x-axis [10].

The boundary conditions which are to be adjoined to Eqs. (1-3) are of mixed type. On the stress-free edges we have the static boundary condition

$$\bar{\sigma}_y = \tau = 0, \quad \text{on } y = \pm b. \tag{4a}$$

On the other hand, the kinematic boundary conditions, according to Fig. 1, are

$$u(\pm L,y) = \mp(u^\circ + \theta^\circ y). \tag{4b}$$

Due to the linearity in the Eqs. (1-3) and boundary conditions (4b), the Principle of Superposition is applicable and it suffices to solve the purely compressive case (θ°=0) and the pure in-plane bending (u°=0) case, separately.

A common method of obtaining the solution to Eqs. (1-3) is based upon the Airy stress function [11]. The resulting fourth order equation is generally solved by separation of variables. The mixed boundary conditions (4a, b) make this approach extremely cumbersome.

An alternative approach involves reformulating the problem in terms of the complementary energy [7,8]

$$\Phi = \frac{1}{2}\int_{-b}^{b}\int_{-L}^{L}[S_{11}\bar{\sigma}_x^2 + 2S_{12}\bar{\sigma}_x\bar{\sigma}_y + S_{22}\bar{\sigma}_y^2$$

$$+S_{44}\bar{\tau}^2]dx\cdot dy$$

$$-\int_{-b}^{b}[u(L,y)\bar{\sigma}_x(L,y)$$

$$+u(-L,y)\bar{\sigma}_x(-L,y)]dy. \qquad (5)$$

The Principle of Minimum Complementary Energy states that of all stress fields ($\bar{\sigma}_x$, $\bar{\sigma}_y$, $\bar{\tau}$) that satisfy the equilibrium equations (1) and the static boundary conditions (4a), the exact solution actually minimize Φ. Thus Eqs. (1-4) may be expressed simply as

$$\delta\Phi = 0.$$

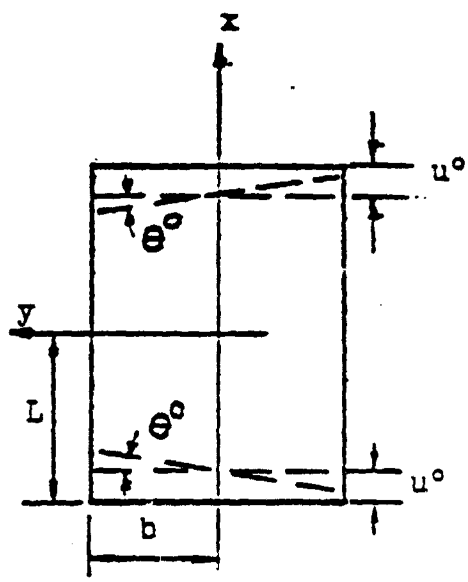

Fig.1 Edge displacements due to perfect gripping and perfect alignment.

Chapter III

FORMAL SOLUTION

A. Pure Compression

Since, in this case, $\theta^\circ = 0$, it is evident that axial stress $\bar{\sigma}_x$ must be an even function of y, and that the shear force along the edges, $x=\pm b$, must vanish. It is therefore clear that the stress $\bar{\sigma}_x$ may be represented by a Fourier series.

$$\bar{\sigma}_x = -\bar{\sigma}_c[1 + \sum_{1}^{N} n \cos\frac{n\pi y}{b} F_n(\frac{\pi x}{b})]. \qquad (6a)$$

For N sufficiently large, and for fixed x, the series will uniformly approximate $\bar{\sigma}_x$ on all intervals for which $\bar{\sigma}_x$ is continuous. At points of discontinuity for $\bar{\sigma}_x$, the series converges to the average value of $\bar{\sigma}_x$. Here, $F_n(\frac{\pi x}{b})$ $(n=1,\ldots N)$ are the unknown Fourier coefficients, and $\bar{\sigma}_c$ is the average compressive stress across every x=constant section.

The remaining stresses $\bar{\sigma}_y$, and $\bar{\tau}$ are obtained by solving the equilibrium equations (1), using the boundary condition (4a). These results are

$$\bar{\sigma}_y = \sigma_c \sum_{1}^{N} \frac{1}{n}\{\cos\frac{n\pi y}{b} + (-1)^{n+1}\} F_n''(\frac{\pi x}{b}), \quad (6b)$$

$$\bar{\tau} = \sigma_c \sum_{1}^{N} \sin\frac{n\pi y}{b} F_n'(\frac{\pi x}{b}). \quad (6c)$$

In deriving Eq. (6c), the vanishing of shear force

$$\int_{-b}^{b} \bar{\tau}(x,y)dy = 0$$

was used to determine the constant of integration. Also $(\ )'$ indicates differentiation with respect to indicated argument.

The unknown functions F_n may be determined by substituting Eqs.(6) into Eq. (5), that is

$$\begin{aligned}
\phi = \frac{1}{2}\cdot\sigma_c^2\cdot\int_{-L}^{L}\int_{-b}^{b}\Big\{ & S_{11}[1+\sum_{1}^{M} m\cos\frac{m\pi y}{b} F_m(\frac{\pi x}{b})] \\
& \cdot[1+\sum_{1}^{N} n\cos\frac{n\pi y}{b} F_n(\frac{\pi x}{b})] \\
& +2S_{12}[1+\sum_{1}^{N} m\cos\frac{m\pi y}{b} F_m(\frac{\pi x}{b})] \\
& \cdot\sum_{1}^{N}\frac{1}{n}[\cos(\frac{n\pi y}{b})+(-1)^{n+1}] F_n'(\frac{\pi x}{b}) \\
& + S_{22}\sum_{1}^{M}\frac{1}{m}[\cos\frac{m\pi y}{b}+(-1)^{m+1}] F_m'(\frac{\pi x}{b}) \\
& \cdot\sum_{1}^{N}\frac{1}{n}[\cos\frac{n\pi y}{b}+(-1)^{n+1}] F_n'(\frac{\pi x}{b})
\end{aligned}$$

$$+S_{44}[\sum_{1}^{M}\sin\frac{m\pi y}{b}F_m'(\frac{\pi x}{b})]\cdot[\sum_{1}^{N}\sin\frac{n\pi y}{b}F_n(\frac{\pi x}{b})]\}dxdy$$

$$+u^{\circ}\sigma_c\int_{-b}^{b}[1+\sum_{1}^{N}n\cos\frac{n\pi y}{b}F_n(\pi\xi)]$$

$$+[1+\sum_{1}^{N}n\cos\frac{n\pi y}{b}F_n(-\pi\xi)]dy\quad, \qquad (7)$$

where $\xi=L/b$.

After intergrating over the y coordinate, application of standard techniques of Variational Calculus [13] renders the expression

$$\delta\Phi = \frac{1}{2}\sigma_c^2\int_{-L}^{L}[-2S_{12}\sum_{1}^{N}F_n''(\frac{\pi x}{b})+3S_{22}\sum_{1}^{N}\frac{1}{n^2}F^{IV}(\frac{\pi x}{b})$$

$$+S_{22}\sum_{1}^{N}F_n(\frac{\pi x}{b})+2S_{22}\sum_{m\neq n}\frac{(-1)^{m+n}}{m\cdot n}F_m^{IV}(\frac{\pi x}{b})$$

$$-S_{44}\sum_{1}^{N}F_n''(\frac{\pi x}{b})]\cdot[\delta F_n(\frac{\pi x}{b})]dx$$

$$+\frac{1}{2}\sigma_c^2[-S_{12}\sum_{1}^{N}F_n(\pm\pi\xi)+2S_{12}\sum_{1}^{N}\frac{(-1)^n}{n}$$

$$+3S_{22}\sum_{1}^{N}\frac{1}{n^2}F_n''(\pm\pi\xi)+2S_{22}\sum_{m\neq n}\frac{(-1)^{m+n}}{m\cdot n}$$

$$\cdot F_m''(\pm\pi\xi)]\cdot[\delta F_n'(\pm\pi\xi)]$$

$$+\frac{1}{2}\sigma_c^2[S_{12}\sum_{1}^{N}F_n'(\pm\pi\xi)-3S_{22}\sum_{1}^{N}\frac{1}{n^2}F_n'''(\pm\pi\xi)$$

$$-2S_{22}\sum_{m\neq n}\frac{(-1)^{m+n}}{m\cdot n}F_m'''(\pm\pi\xi)$$

$$+\ S_{44}\sum_{1}^{N}F_n'(\pm\pi\xi)]\cdot[\delta F_n(\pm\pi\xi)]$$

$$=0. \tag{8}$$

It immediately follows from (8) that the Euler equations are

$$\sum_{1}^{N}[S_{22}\frac{3}{n^2}F_n^{IV}(\frac{\pi x}{b})-(2S_{12}+S_{44})F_n''(\frac{\pi x}{b})+S_{22}F_n(\frac{\pi x}{b})]$$

$$+\sum_{m\neq n}[2S_{22}\frac{(-1)^{m+n}}{m\cdot n}F_m^{IV}(\frac{\pi x}{b})]$$

$$=0. \tag{9a}$$

and the natural boundary conditions are

$$\sum_{1}^{N}[S_{22}\frac{3}{n^2}F_n''(\pm\pi\xi)-S_{12}F_n(\pm\pi\xi)]$$

$$+\sum_{m\neq n}[2S_{22}\frac{(-1)^{m+n}}{m\cdot n}F_m''(\pm\pi\xi)]$$

$$=\sum_{1}^{N}[2S_{22}(-1)^{n+1}/n], \tag{9b}$$

$$\sum_{1}^{N}[(S_{44}+S_{12})F_n'(\pm\pi\xi)-S_{22}\frac{3}{n^2}F_n'''(\pm\pi\xi)]$$

$$-\sum_{m\neq n}[2S_{22}\frac{(-1)^{m+n}}{m\cdot n}F_m'''(\pm\pi\xi)]$$

$$=0. \tag{9c}$$

With the introduction of the following definitions:

$$S_{11} = 1/E_x, \quad S_{12} = -\nu_{xy}/E_x = -\nu_{yx}/E_x,$$

$$S_{22} = 1/E_y, \quad S_{44} = 1/G_{xy},$$

$$\Gamma_o = (2S_{12} + S_{44})/S_{22} = E_y/G_{xy} - 2\nu_{yx},$$

$$\underset{\sim}{M} = \begin{bmatrix} \frac{3}{1^2} & \frac{2}{1}(\frac{-1}{2}) & \frac{2}{1}(\frac{+1}{3}) & - & + & \cdot & \cdot \\ & \frac{3}{2^2} & \frac{2}{2}(\frac{-1}{3}) & + & - & \cdot & \cdot \\ & & \frac{3}{3^2} & \cdot & \cdot & \cdot & \cdot \\ & & & \cdot & \cdot & \cdot & \cdot \\ \text{Sym.} & & & & & & \frac{3}{N^2} \end{bmatrix},$$

$$\underset{\sim}{K} = \begin{bmatrix} 1^2 & & & & \\ & 2^2 & & 0 & \\ & & 3^2 & & \\ & 0 & & \cdot & \\ & & & & N^2 \end{bmatrix} \cdot E_y/E_x,$$

$$\underset{\sim}{I} = \begin{bmatrix} 1 & & & 0 \\ & 1 & & \\ & & \cdot & \\ 0 & & & \cdot \\ & & & & 1 \end{bmatrix}, \qquad \underset{\sim}{F} = \begin{bmatrix} F_1 \\ F_2 \\ \vdots \\ \cdot \\ F_N \end{bmatrix},$$

$$H_n = (-1)^{n+1}/n, \quad \underset{\sim}{H} = [H_1 \; H_2 \; \cdot \; \cdot \; H_N]^T$$

Eqs. (9a, b, c) may be conveniently cast in the form

$$\underset{\sim}{M}\,\underset{\sim}{F}^{IV} - \Gamma_o\,\underset{\sim}{1}\,\underset{\sim}{F}'' + \underset{\sim}{K}\,\underset{\sim}{F} = 0, \qquad (10a)$$

and

$$\underset{\sim}{M}\,\underset{\sim}{F}_n''(\pm\pi\xi) + \nu_{yx}\,\underset{\sim}{1}\,\underset{\sim}{F}_n(\pm\pi\xi) = 2\nu_{yx}\underset{\sim}{H}, \qquad (10b)$$

$$(\Gamma_o + \nu_{xy})\,\underset{\sim}{1}\,F_n'(\pm\pi\xi) - \underset{\sim}{M}\,F_n'''(\pm\pi\xi) = 0. \qquad (10c)$$

It is also necessary to determine the constant σ_c. After differentiating Φ (Eq. 7) with respect to σ_c and simplifying the resulting expression with the aid of Eqs.(9a,b,c) and setting

$$\frac{\partial\Phi}{\partial\sigma_c} = 0,$$

we obtain

$$u^e = \frac{\sigma_c L}{E_x}\left[1 - \frac{\nu_{xy}}{\pi\xi}\sum_1^N \frac{1}{n}(-1)^n F_n'(\pi\xi)\right]. \qquad (11)$$

It should be noted that if $F_n=0$ $(n=1, \ldots N)$, then Eq. (11) reduces to the elementary strength of materials formula [12].

The solutions for N terms retained in the series (6), and the solutions to Eqs. (9a, b, c) give the "best" (in the mean square sense) N-term approximation to the true solution. Therefore, it is reasonable to expect that the approximate stresses will be closest to their true values at locations where their true values are the largest, that is, at the constrained edges.

Eq. (10a) is a fourth order ordinary differential equation with constant coefficients. Thus, we assume a solution of the form

$$\underline{F} = \underline{\eta} \cosh(\alpha\pi x/b). \qquad (12)$$

Substitution of Eq. (12) into (10a) generates the eigenvalue problem:

$$[\alpha^4 \underline{M} - \alpha^2 \Gamma_o \underline{1} + \underline{K}]\, \underline{\eta} = 0 \qquad (13)$$

for the eigenvalues α and eigenvectors $\underline{\eta}$.

Note that α and $\underline{\eta}$ are obtained independent of the boundary conditions, and hence they do not depend upon the manner in which the compression load is introduced. They depend only upon the number of terms N retained in the series, and the material constant Γ_o. In the case of quasi-isotropic $[0/\pm45/90]_s$ layups, $\Gamma_o = 2$, and they are also independent of the material constants.

A necessary and sufficient condition for the existence of a non-trivial solution to Eq. (13) is

$$\det[\alpha^4 \underline{M} - \alpha^2 \Gamma_o \underline{1} + \underline{K}] = 0 \qquad (14)$$

Eq. (14) is a polynomial of order 4N; however all solutions must occur in equal and opposite pairs. And if the roots are complex, they must also occur in pairs of complex conjugates.

If, for complex eigenvalues, the components of the p-th eigenvector are assumed as

$$\underline{\eta}_p = A_p\ [1\ \eta_{p2} \cdot\cdot\cdot \eta_{pN}],$$

then the general solution to Eq. (10a) for even functions F_n becomes

$$F_n = \sum_{p=1}^{N} \{A_p\ \eta_{pn} \cosh(\alpha_p \pi x/b)$$

$$+\bar{A}_p\ \bar{\eta}_{pn} \cosh(\bar{\alpha}_p \pi x/b)$$

$$= 2\cdot\mathrm{Re}\{\sum_{p=1}^{N} A_p\ \eta_{pn} \cosh(\alpha_p \pi x/b) \qquad (15a)$$

where bars above the symbols indicate complex conjugate.

For real eigenvalues α_p^1, α_p^2 $(p=1,2,\cdot\cdot\cdot N)$ the general solution is

$$F_n = \sum_{p=1}^{N} [A_p^1\ \eta_{pn}^1\ \cosh(\alpha_p^1 \pi x/b)$$

$$+\ A_p^2\ \eta_{pn}^2\ \cosh(\alpha_p^2 \pi x/b)], \qquad (15b)$$

where

$$\underline{\eta}_{pn}^1 = A_p^1\ [1\ \eta_{p2}^1\ \eta_{p3}^1 \cdot\cdot\cdot \eta_{pN}^1],$$

$$\underline{\eta}_{pn}^2 = A_p^2\ [1\ \eta_{p2}^2\ \eta_{p3}^2 \cdot\cdot\cdot \eta_{pN}^2].$$

The complex constants A_p or real constants A_p^1 and A_p^2 are determined from the boundary conditions (10b, c).

The remaining possibility that some roots are real and some complex was not encountered in the numerical calculations for the assumed data. Thus, although this case is as routine as the two foregoing cases, it will not be discussed further.

B. Pure in-plane Bending

For pure bending, $u^\circ=0$, and the axial stress is an odd function of y. As before, the shear force along the edges $x=\pm b$ must vanish. However, it turns out that a Fourier Sine series approximation to $\bar{\sigma}_x$ is not convenient. This is because application of the boundary conditions (4a) to the stresses obtained after integrating Eqs. (1) introduces side constraints on the Fourier coefficients. In order to circumvent this difficulty, $\bar{\sigma}_x$ is expanded in terms of odd Legendre polynomials.

One definition of the N-th Legendre polynomial is [13]

$$P_n\left(\frac{y}{b}\right) = \sum_{k=0}^{N} \frac{(-1)^k\,(2n-2k)!}{2^n k!\,(n-k)!\,(n-2k)!}\left(\frac{y}{b}\right)^{n-2k},$$

where $N=\frac{n}{2}$ n: even

$$N=\frac{(n-1)}{2} \quad n:\ \text{odd}\,. \tag{16}$$

Then the stress $\bar{\sigma}_x$ may be represented by

$$\bar{\sigma}_x = -\sigma_b \left[P_1\left(\frac{y}{b}\right) + \sum_{3,5,\cdots}^{N} P_n\left(\frac{y}{b}\right) \right] G_n\left(\frac{x}{b}\right). \qquad (17a)$$

Here, $G_n(\frac{x}{b})$ are the unknown generalized Fourier coefficients, and σ_b is a constant.

The remaining stresses $\bar{\sigma}_y$, and $\bar{\tau}$ are obtained by solving the equilibrium equations (1) subject to the boundary condition (4a). These results are

$$\bar{\sigma}_y = -\sigma_b \sum_{3,5,\cdots}^{N} \left[\frac{P_{n-2}\left(\frac{y}{b}\right)}{(2n+1)(2n-1)} - \frac{2P_n\left(\frac{y}{b}\right)}{(2n-1)(2n+3)} + \frac{P_{n+2}\left(\frac{y}{b}\right)}{(2n+1)(2n+3)} \right] G_n''\left(\frac{x}{b}\right), \qquad (17b)$$

$$\bar{\tau} = -\sigma_b \sum_{3,5,\cdots}^{N} \frac{1}{(2n+1)} \left[P_{n-1}\left(\frac{y}{b}\right) - P_{n+1}\left(\frac{y}{b}\right) \right] G_n'\left(\frac{x}{b}\right). \qquad (17c)$$

In deriving Eq. (17c), the vanishing of shear force

$$\int_{-b}^{b} \bar{\tau}(x,y)dy = 0$$

was used to determine the constant of integration. Also $(\ )'$ denotes differentiation with respect to the indicated argument.

The unknown functions G_n may be determined by substituting Eq. (17) into Eq. (5), and integrating over the y-coordinate. After applying the variational method and collecting terms, the Euler equations are obtained:

$$\underset{\sim}{M}\, G^{IV} - \Gamma_0\, \underset{\sim}{C}\, G'' + \underset{\sim}{K}\, G = 0 \qquad (18)$$

where

$$M = \begin{bmatrix} \frac{6}{3\cdot5\cdot7\cdot9\cdot11} & \frac{-4}{5\cdot7\cdot9\cdot11\cdot13} & \frac{1}{7\cdot9\cdot11\cdot13\cdot15} & 0 \\ & \frac{6}{7\cdot9\cdot11\cdot13\cdot15} & \frac{-4}{9\cdot11\cdot13\cdot15\cdot17} & \cdot \\ & & \cdot & \cdot \\ & & & M(N-2,N) \\ & \text{Sym.} & & M(N-1,N) \\ & & & M(N,N) \end{bmatrix}$$

$$M(N,N) = \frac{6}{(2N-3)(2N-1)(2N+1)(2N+3)(2N+5)},$$

$$M(N-1,N) = \frac{-4}{(2N-5)(2N-3)(2n-1)(2N+1)(2N+3)},$$

$$M(N-2,N) = \frac{1}{(2N-7)(2N-5)(2N-3)(2N-1)(2N+1)},$$

$$C = \begin{bmatrix} \frac{2}{5\cdot7\cdot9} & \frac{-1}{7\cdot9\cdot11} & & 0 \\ & \frac{2}{9\cdot11\cdot13} & \frac{-1}{11\cdot13\cdot15} & \\ & & \cdot & \cdot \\ & & & \frac{-1}{(2N-3)(2N-1)(2N+1)} \\ & & & \frac{2}{(2N-1)(2N+1)(2N+3)} \end{bmatrix},$$

$$\underset{\sim}{K} = \begin{bmatrix} \frac{1}{7} & & & \\ & \frac{1}{11} & & 0 \\ & & \ddots & \\ 0 & & & \frac{1}{(2N+1)} \end{bmatrix} . E_y/E_x \quad , \quad \underset{\sim}{G} = \begin{bmatrix} G_3 \\ G_5 \\ \cdot \\ \cdot \\ \cdot \\ G_N \end{bmatrix}$$

The natural boundary conditions associated with Eq. (18) are

$$\underset{\sim}{M}\,\underset{\sim}{G}''\,(\pm\xi) + \nu_{xy}\,\underset{\sim}{C}\,\underset{\sim}{G}\,(\pm\xi) = \frac{\nu_{yx}}{105}[\,1\;0\;0\;.\;.\;0]^T\,, \tag{19a}$$

$$\underset{\sim}{M}\,\underset{\sim}{G}'''\,(\pm\xi) - (\Gamma_o+\nu_{yx})\underset{\sim}{C}\,\underset{\sim}{G}'\,(\pm\xi) = 0\,. \tag{19b}$$

In addition, the condition $\frac{d\phi}{d\sigma_b}=0$ results in, after considerable manipulations,

$$\theta^o = \frac{3M_b\xi}{E_x \cdot 2b^2}\,[\,1 - \frac{\nu_{xy}}{35\xi}\,G_3'\,(\xi)]\,, \tag{20}$$

where

$$M_b = -\int_{-b}^{b} y\,\sigma_x\,dy = \frac{2}{3}\,\sigma_b\,b^2\,.$$

It should be noted that in Bernoulli-Euler theory

$$\theta^o = \frac{3M_b\xi}{E_x \cdot 2b^2}\,. \tag{21}$$

The method of solving Eqs. (18, 19) is the same as in the pure compression problem. We write

$$\underset{\sim}{G} = \underset{\sim}{\zeta} \cosh(\frac{\beta x}{b}) \;,$$

where β and $\underset{\sim}{\zeta}$ are the eigenvalues and eigenvectors, respectively. Thus β and $\underset{\sim}{\zeta}$ are determined from

$$[\beta^4 \underset{\sim}{M} - \beta^2 \Gamma_o \underset{\sim}{C} + \underset{\sim}{K}] \underset{\sim}{\zeta} = 0 \;. \qquad (22)$$

If the components of the complex eigenvectors are

$$\zeta_p = B_p \, [1 \;\; \zeta_{p2} \;\; \cdot \;\; \cdot \;\; \cdot \;\; \zeta_{pN}],$$

the solution for G_n is given by

$$G_n = 2 \cdot \mathrm{Re} \, \{ \sum_{p=1}^{N} B_p \, \underset{\sim}{\zeta} \cosh(\frac{\beta_p x}{b}) \} \;.$$

For real eigenvalues, the counterpart to Eq. (15b) is

$$G_n = \sum_{p=1}^{N} [\, B_p^1 \, \zeta_{pn}^1 \cosh(\frac{\beta_p^1 x}{b}) + B_p^2 \, \zeta_{pn}^2 \cosh(\frac{\beta_p^2 x}{b})] . \qquad (23b)$$

C. Lamina Stress

In the previous two sections (A, B), we formally obtained approximate solutions for the average stress and as a consequence of Eqs. (3), strain. The remaining task is now to obtain the stresses within each constituent lamina. The approach here will follow Jones [10].

For either quasi-isotropic or cross-ply laminates, the stress-strain relations (3) may be written

$$\begin{Bmatrix} \epsilon_x \\ \epsilon_y \\ \frac{\gamma_{xy}}{2} \end{Bmatrix} = \begin{bmatrix} \frac{1}{E} & \frac{-\nu}{E} & 0 \\ \frac{-\nu}{E} & \frac{1}{E} & 0 \\ 0 & 0 & \frac{1}{2G} \end{bmatrix} \begin{Bmatrix} \bar{\sigma}_x \\ \bar{\sigma}_y \\ \bar{\tau} \end{Bmatrix} = [Q] \begin{Bmatrix} \bar{\sigma}_x \\ \bar{\sigma}_y \\ \bar{\tau} \end{Bmatrix} \quad (24)$$

where E is the Young's modulud ($E_x = E_y = E$), ν is the Poisson's ratio ($\nu_{xy} = \nu_{yx} = \nu$), and G is the shear modulus ($G_{xy} = G_{yx} = G$). Each constituent lamina of thelaminate sustains the same strain $[\epsilon_x, \epsilon_y, \frac{\gamma_{xy}}{2}]^T$ in the x-y coordinate system.

However, the stresses differ from one lamina to the next. It is necessary, therefore, to determine the appropriate stress-strain relation for each lamina. Let us suppose that the principal material axes are inclined at an angle θ to the x-axis (see Fig. 2). Then the strains in the material coordinates are obtained from the laminate strain by

$$\begin{Bmatrix} \epsilon_1 \\ \epsilon_2 \\ \frac{\gamma_{12}}{2} \end{Bmatrix} = [T] \begin{Bmatrix} \epsilon_x \\ \epsilon_y \\ \frac{\gamma_{xy}}{2} \end{Bmatrix}, \qquad [T] = \begin{bmatrix} \cos^2\theta & \sin^2\theta & \sin 2\theta \\ \sin^2\theta & \cos^2\theta & -\sin 2\theta \\ \frac{-\sin 2\theta}{2} & \frac{\sin 2\theta}{2} & \cos 2\theta \end{bmatrix}$$

(25)

Similarly, the stresses in the principal coordinates are given by

$$\begin{Bmatrix} \sigma_1 \\ \sigma_2 \\ \tau_{12} \end{Bmatrix} = [T] \begin{Bmatrix} \sigma_x \\ \sigma_y \\ \tau_{xy} \end{Bmatrix} . \qquad (26)$$

Now let the constitutive equation in the 1-2 principal coordinate system be

$$\begin{Bmatrix} \sigma_1 \\ \sigma_2 \\ \tau_{12} \end{Bmatrix} = [S] \begin{Bmatrix} \varepsilon_1 \\ \varepsilon_2 \\ \frac{\gamma_{12}}{2} \end{Bmatrix} , \qquad (27)$$

$$[S] = \begin{bmatrix} \frac{E_1}{1-\nu_{12}\nu_{21}} & \frac{\nu_{12}E_2}{1-\nu_{12}\nu_{21}} & 0 \\ \frac{\nu_{21}E_1}{1-\nu_{12}\nu_{21}} & \frac{E_2}{1-\nu_{12}\nu_{21}} & 0 \\ 0 & 0 & 2G_{12} \end{bmatrix} ,$$

where E_1, E_2 are Young's moduli in the 1 and 2 directions, respectively, ν_{12} is Poisson's ratio for stresses applied in the fiber direction, $\nu_{21} = \nu_{12}E_2/E_1$, and G_{12} is the principal shear modulus.

After combining Eqs. (24, 25, 26, 27), we obtain

$$\begin{Bmatrix} \sigma_x \\ \sigma_y \\ \tau_{xy} \end{Bmatrix} = [T]^{-1}[S][T][Q] \begin{Bmatrix} \bar{\sigma}_x \\ \bar{\sigma}_y \\ \bar{\tau}_{xy} \end{Bmatrix} , \qquad (28)$$

where

$$[T]^{-1} = \begin{bmatrix} \cos^2\theta & \sin^2\theta & -\sin 2\theta \\ \sin^2\theta & \cos^2\theta & \sin 2\theta \\ \frac{\sin\theta}{2} & \frac{-\sin\theta}{2} & \cos 2\theta \end{bmatrix}$$

Following fundamental matrix algebra, Eq. (28) can be simplified to the form

$$\begin{Bmatrix} \sigma_x \\ \sigma_y \\ \tau_{xy} \end{Bmatrix} = [C] \begin{Bmatrix} \bar{\sigma}_x \\ \bar{\sigma}_y \\ \bar{\tau} \end{Bmatrix} , \qquad (29)$$

where

$$[C] = [T]^{-1} \cdot [S] \cdot [T] \cdot [Q].$$

Clearly, the matrix [C] depends upon the lamina material properties and orientation.

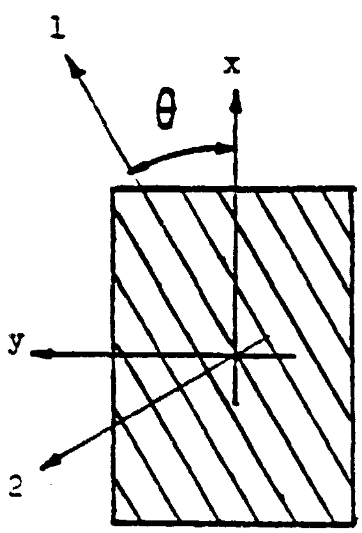

Fig. 2 Principal material coordinate systems.

Chapter IV

NUMERICAL SOLUTION TO THE EIGENVALUE PROBLEM

We now take up the numerical solution to the polynomial of order 4N

$$f(\alpha) = \det [\alpha^4 \underset{\sim}{M} - \alpha^2 \Gamma_o \underset{\sim}{C} + \underset{\sim}{K}] = 0 \cdot$$

Clearly $f(\alpha)$ has the form

$$f(\alpha) = C_1\alpha^{4N} + C_2\alpha^{4N-2} + \ldots + C_N\alpha^2 + C_{N+1} ,$$

where C_i are functions of certain invariants of the matrices $\underset{\sim}{M}$, $\underset{\sim}{C}$ and $\underset{\sim}{K}$ and their products. For example, C_{N+1}=det [K] and C_1=det [M]. The other coefficients, however, are considerably more involved.

A numerical method for determining the set of C_i's for given N relies on the utilization of a high capacity computer. By reasonably choosing a set of arbitrary numbers ($\alpha_1', \alpha_2', \ldots \alpha_{N+1}'$) and evaluating $f(\alpha_i')$ N+1 times, we obtain the simultaneous equations

$$C_1\ (\alpha_1')^{4N} + C_2\ (\alpha_1')^{4N-2} + \ldots + C_{N+1} = f(\alpha_1')$$

$$C_1\ (\alpha_2')^{4N} + C_2\ (\alpha_2')^{4N-2} + \ldots + C_{N+1} = f(\alpha_2')$$

. . . .

. . . .

$$C_1(\alpha'_{N+1})^{4N} + C_2(\alpha'_{N+1})^{4N-2} + \cdots + C_{N+1} = f(\alpha'_{N+1})$$

The coefficients C_i may now be routinely obtained by solving the above set of simultaneous equations in which C_i's are the unknowns. The numerical sensitivity of the procedure may be checked by choosing several different sets $\{\alpha'_i\}$ and comparing the solutions. Furthermore, in our case, it is convenient to reduce the order of the polynomial from 4N to 2N, by taking $(\alpha'_i)^{1/2}$ instead of α'_i. This step also speeds up the process of obtaining the roots of the polynomial. These roots, i.e. the eigenvalues, were obtained by using a standard subroutine based on the Newton-Raphson method.[14].

The eigenvectors are determined from a set of linear algebraic equations (13 or 22). Since the eigenvectors are not unique, a very convenient normalization procedure is to set the first component of each eigenvector equal to unity. The coefficients A_p, determined by the natural boundary conditions, are also routinely obtained by solving a set of linear algebraic equations.

Chapter V

NUMERICAL RESULTS

A. Pure Compression

a. Quasi-Isotropic (Q-I) $[0/\pm 45/90]_s$ Laminates

1. Generalized Plane Stress

According to elementary rod theory, the stresses, sufficiently far from the edges at which the load is instroduced, are assumed to be uniaxial, i.e.

$$\bar{\sigma}_x = -\sigma_c = \frac{-u^o E_x}{L}, \quad \bar{\sigma}_y = \bar{\tau} = 0. \qquad (30)$$

Thus the specimen must have a sufficiently long gage length if Eq. (30) is to be applicable anywhere. Elementary theory, however, is able to provide neither the minimum gage length necessary for Eq. (30) to hold nor the stresses in the neighborhood of the clamped edges.

In the present approach, the general plane stresses $\bar{\sigma}_x$, $\bar{\sigma}_y$ & $\bar{\tau}_{xy}$ depend upon the material constants ν_{yx}, E_y/E_x and Γo, and the specimen geometry ratio ξ.

For quasi-isotropic laminates, $\Gamma_o=2$, $E_x=E_y$, and hence the stress distributions merely depend upon ν and ξ.

The stresses were calculated for a range of ξ from 1/4 to 6, and for $\nu=0.336$* which is a fairly typical value for graphite/epoxy quasi-isotropic laminates. It will be noted from Eqs.(10) that the stresses are approximately propotional to ν and therefore approximate solution for other Poisson ratio's may be obtained by scaling the current solution.

Since $\Gamma_o=2$ for all Q-I laminates, the eigenvalues α_i $(i=1,2,\cdots,N)$ computed from Eq.(14) merely depend upon the number of terms, N, retained in the series [Eqs.(6)]. The results of this computation, as explained in Ch. III, are shown in Table 1 for values of N ranging from 1 to 10. It will be noted that all the eigenvalues for $n\leq10$ are complex values, and consequently the solutions for the functions F_n $(n=1,2,\cdots,N)$ are given by Eq. (15).

The stresses [Eqs. (6)] were plotted for different values of N at various cross-sections x/L = constant in order to assess convergence for increasing N.

---

* This values was obtained for the material properties:
$E_1=21\times10^3$ ksi, $E_2=1.7\times10^3$ ksi, $\nu_{12}=0.4$,
$G_{12}=0.65\times10^3$ ksi, $E=7.95\times10^3$ ksi.

TABLE 1. Eigenvalues for Q-I laminate in pure compression

N \ α		1	2	3	4	5	6	7	8	9	10
1	Re	0.67	0.67	0.67	0.67	0.67	0.67	0.67	0.67	0.67	0.67
	Im	0.35	0.36	0.36	0.36	0.36	0.36	0.36	0.36	0.36	0.36
2	Re		1.70	1.70	1.70	1.70	1.70	1.70	1.70	1.70	1.70
	Im		0.46	0.48	0.49	0.49	0.49	0.49	0.49	0.49	0.49
3	Re			2.70	2.70	2.71	2.71	2.71	2.72	2.72	2.72
	Im			0.51	0.55	0.56	0.56	0.56	0.56	0.56	0.56
4	Re				3.70	3.71	3.71	3.71	3.72	3.72	3.72
	Im				0.53	0.58	0.60	0.61	0.61	0.61	0.62
5	Re					4.68	4.69	4.71	4.71	4.72	4.72
	Im					0.55	0.61	0.63	0.64	0.65	0.65
6	Re						5.68	5.69	5.70	5.71	5.71
	Im						0.57	0.63	0.66	0.67	0.67
7	Re							6.67	6.68	6.70	6.71
	Im							0.57	0.65	0.68	0.69
8	Re								7.66	7.67	7.69
	Im								0.58	0.66	0.69
9	Re									8.66	8.67
	Im									0.59	0.67
10	Re										9.65
	Im										0.59

As shown in Figs.(4,6–8), convergence was excellent away from the constrained edges with just three terms retained in the series. Near, but not at the clamped edges, convergence was excellent with only six terms retained in the Fourier series solutions [see Fig. 5, 14]. Another measure of the convergence is provided by Eq. (11). In Table 2 the ratio u^oE_x/σ_cL was evaluated for various values of N and ξ.

The convergence of u^oE_x/σ_cL for increasing N is evident from Table 2. Note that for large ξ, the value approaches unity, which is the result predicted from elementary rod theory, Eq. (30). The reciprocal of the entries in Table 2 represents the apparent percentage increase in average stiffness due to the constrained edges.

It is convenient to write the generalized plane stresses in the form

$$\begin{aligned} \bar{\sigma}_x &= -\sigma_c[1+\delta_x(x,y)], \\ \bar{\sigma}_y &= \sigma_c\delta_y(x,y), \qquad (31) \\ \bar{\tau}_{xy} &= \sigma_c\delta_{xy}(x,y). \end{aligned}$$

Clearly, for $|\delta_x|$, $|\delta_y|$ and $|\delta_{xy}|$ sufficiently small, Eq. (31) will closely approximate Eq. (30). We shall say that the stress state is approximately uniaxial

TABLE 2. Values of $u^{\circ}E_x/\sigma_c L$ for Q-I laminate in pure compression

$u^{\circ}E_x/\sigma_c L$						
N \ ξ	0.25	0.50	1	3	6	
1	0.9342	0.9545	0.9770	0.9926	0.9963	
3	0.9203	0.9443	0.9714	0.9907	0.9954	
5	0.9173	0.9422	0.9702	0.9903	0.9952	
6	0.9166	0.9417	0.9699	0.9902	0.9951	
7	0.9161	0.9413	0.9697	0.9902	0.9951	

at a given x=constant cross-section if

$$|\delta_x| \leq 0.02$$
$$|\delta_y| \leq 0.02 \qquad \text{for } |y| \leq b \qquad (32)$$
$$|\delta_{xy}| \leq 0.02$$

The 2% bound on the deviation of the true stresses from the uniaxial state is, although arbitrary, quite useful particularly for the experimentalist. By providing a definite bound, the effect of the constrained edge can be quantified.

For geometry ratio's $\xi<1.5$, (32) was not satisfied anywhere. Thus the effect of the constrained edges is observed everywhere in the specimen. Stresses distributions along the center line $x=0$ and at the edge $x=L$ are shown in Figs. 6-11 for $\xi=1/4$, $\xi=1/2$, and $\xi=1$, respectively.

For $\xi>1.5$, there exists a region in which the stress state is approximately uniaxial, i.e. Eq. (32) is satisfied. It was found that the domain of influence of the edge is limited to 1.5b (or 75% of the width), as depicted in Fig. 3.

As expected, the stresses in the shaded region of Fig. 3 are independent of ξ provided $L>1.5b$. Consequently, once the stresses are determined for one value of $\xi>1.5$, they are known for all values $\xi>1.5$.

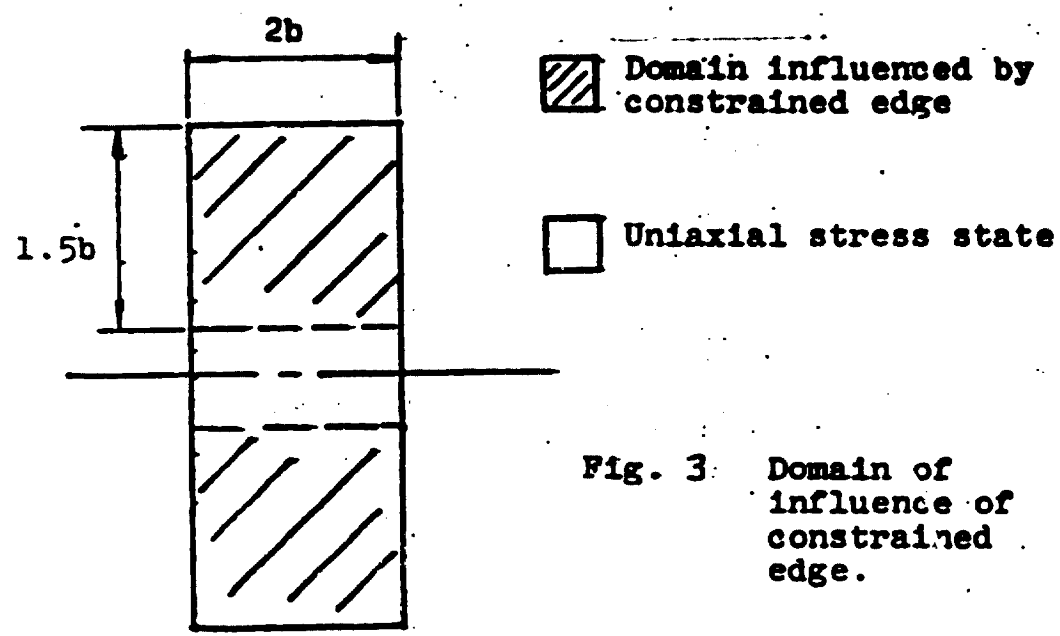

Fig. 3 Domain of influence of constrained edge.

Increasing L, for fixed b, merely increases the uniaxial stress domain. Results are shown in Figs.(4,5,12) for $\xi=3$ and $x/L=0.75$, 0.9 and 1.0 respectively. According to the foregoing discussion, the generalized stresses are the same for $\xi=6$ and $x/L=0.875$, 0.95 and 1, respectively [Figs. 13-15]

It should be observed that the stresses at the edge $x=L$ for $\xi=1$ [Fig.11] and $\xi=3$ [Fig.12] are almost identical. The reason for this is because the stresses at $x=L$ are affected by the constrained condition at only that edge; the stresses at each edge $x=\pm L$ for both $\xi=1$ and $\xi=3$ are outside the domain of influence of the other edge $x=\mp L$.

As indicated earlier, the stresses at the clamped edge appeared to be converging [Fig.12] quite well for N=6. A closer examination of the tabulated values of $\bar{\sigma}_x(L,y)$ did indeed confirm convergence for $|y|<b$. However, at the corners $y=b$, the stress $\bar{\sigma}_x$ appears to grow without bound. This apparent singularity is shown in Table 3.

2. Lamina Stress

Figures 16-18 show representative laminae stress at the constrained edge of Q-I laminate for the plies

TABLE 3. Normalized stress at corners $\sigma_x(L,b)/\sigma_c$ for Q-I laminate in pure compression

$\sigma_x(L,b)/\sigma_c$						
N \ ξ	0.25	0.50	1	3	6	
1	0.97	1.05	1.12	1.13	1.13	
2	1.01	1.13	1.22	1.23	1.23	
3	1.05	1.20	1.31	1.31	1.31	
4	1.09	1.27	1.38	1.38	1.38	
5	1.13	1.33	1.44	1.44	1.44	
6	1.18	1.38	1.45	1.50	1.50	
7	1.21	1.42	1.50	1.55	1.55	
8	1.24	1.47	1.55	1.60	1.60	
9	1.27	1.51	1.59	1.64	1.64	
10	1.30	1.55	1.63	1.68	1.68	

STRESS DISTRIBUTION DIAGRAM

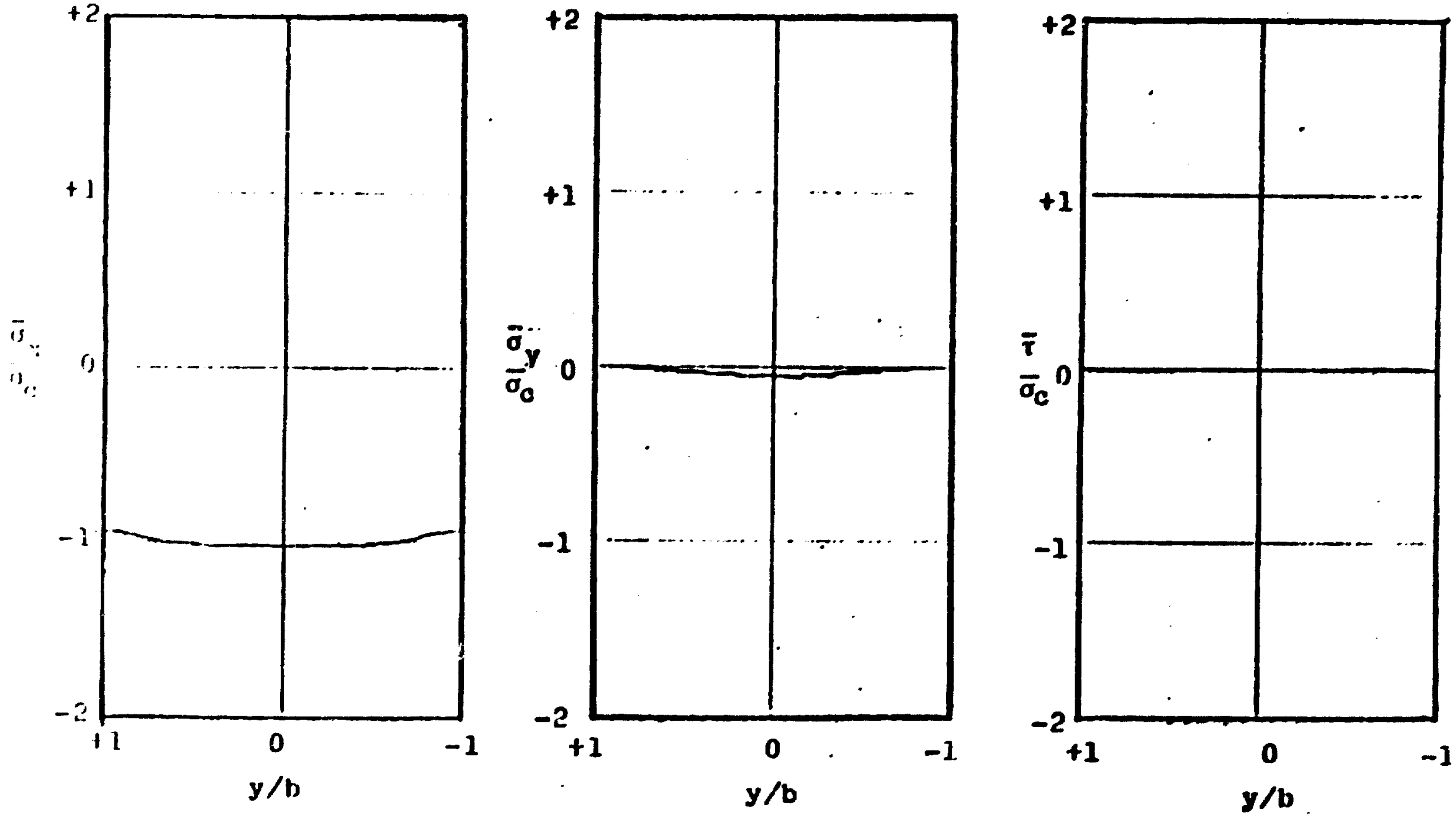

Figure 4 Compression, Q-I laminate, ξ=3,x/L=0.75, N=3,4

STRESS DISTRIBUTION DIAGRAM

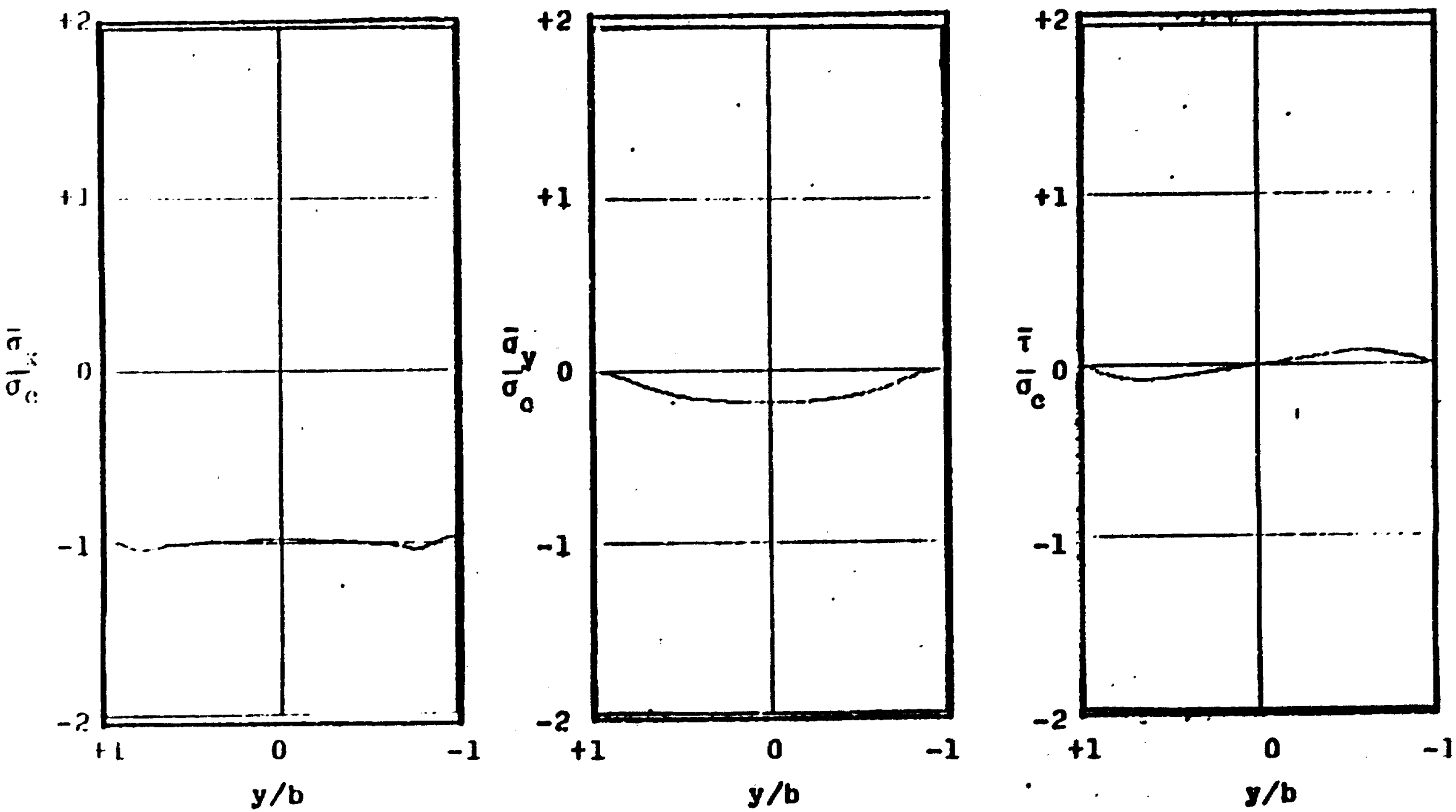

Figure 5 Compression, Q-I laminate, $\xi = 3$, $x/L = 0.9$, $N = 6,7$

STRESS DISTRIBUTION DIAGRAM

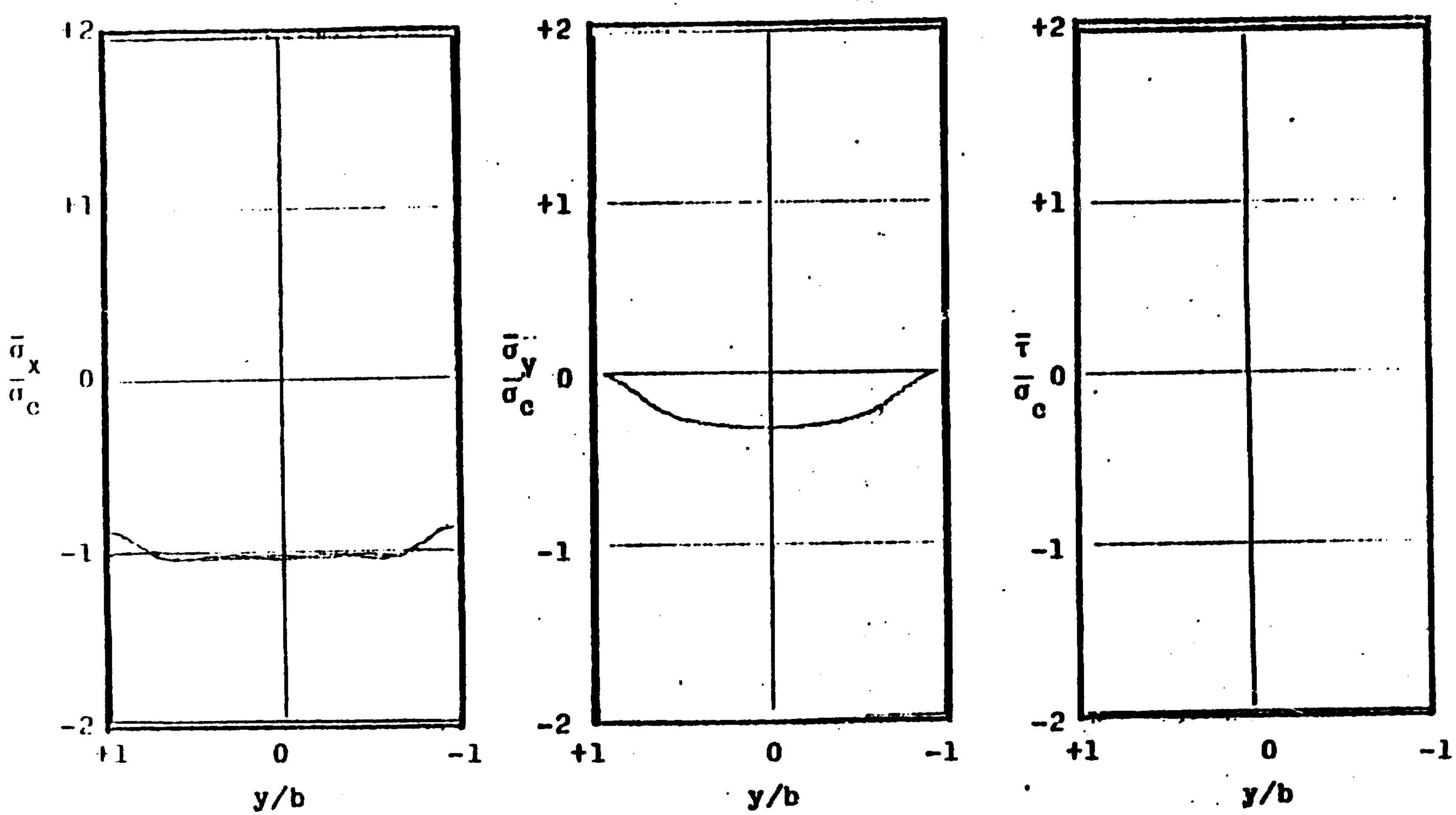

Figure 6 Compression, Q-I laminate, $\xi=1/4$, $x/L=0$, $N=3,4$

STRESS DISTRIBUTION DIAGRAM

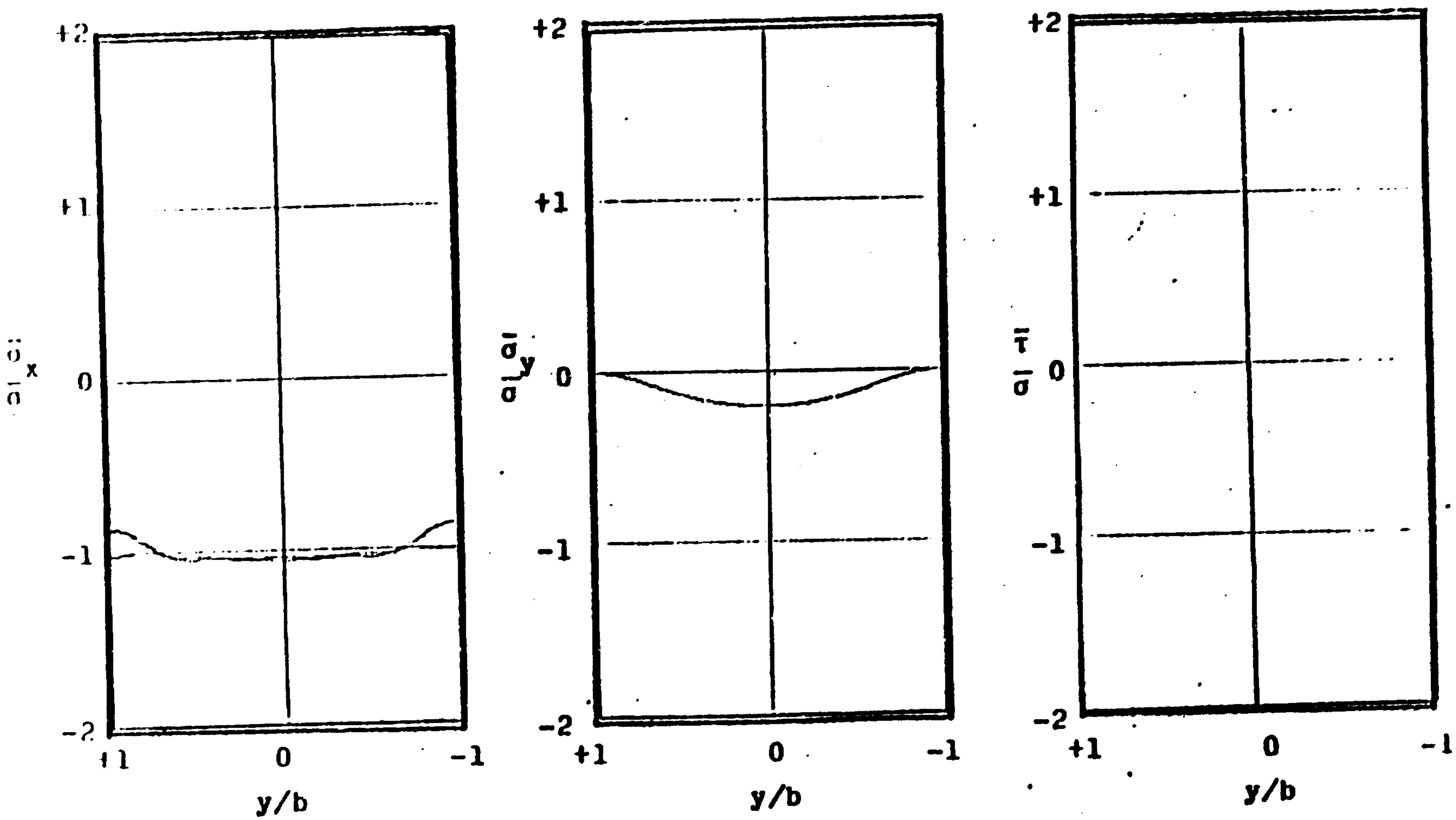

Figure 7 Compression, 0-I laminate, $\xi=1/2$, $x/L=0$, $N=3,4$

STRESS DISTRIBUTION DIAGRAM

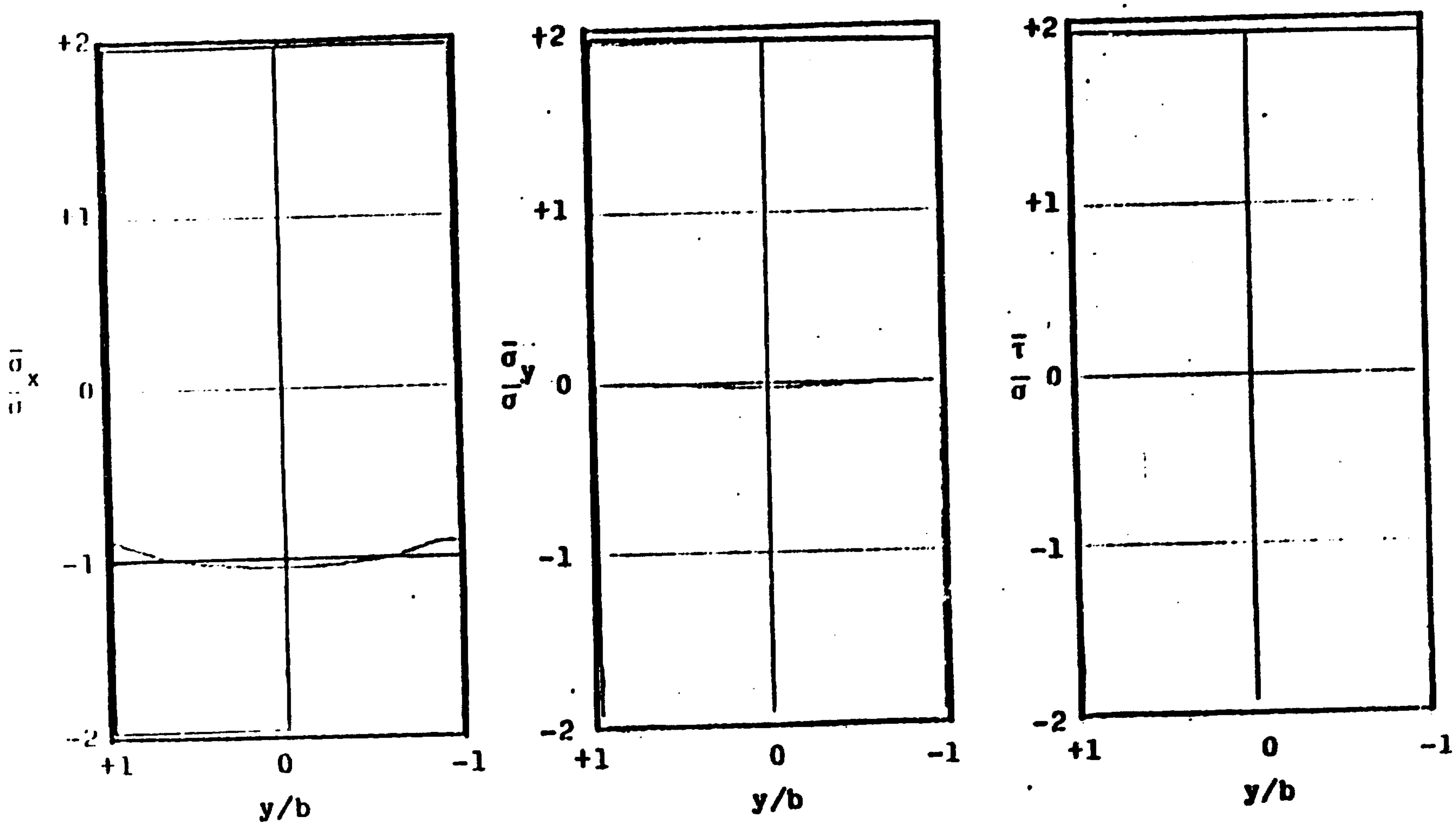

Figure 8 Compression, Q-I laminate, ξ=1, x/L=0, N=3,4

STRESS DISTRIBUTION DIAGRAM

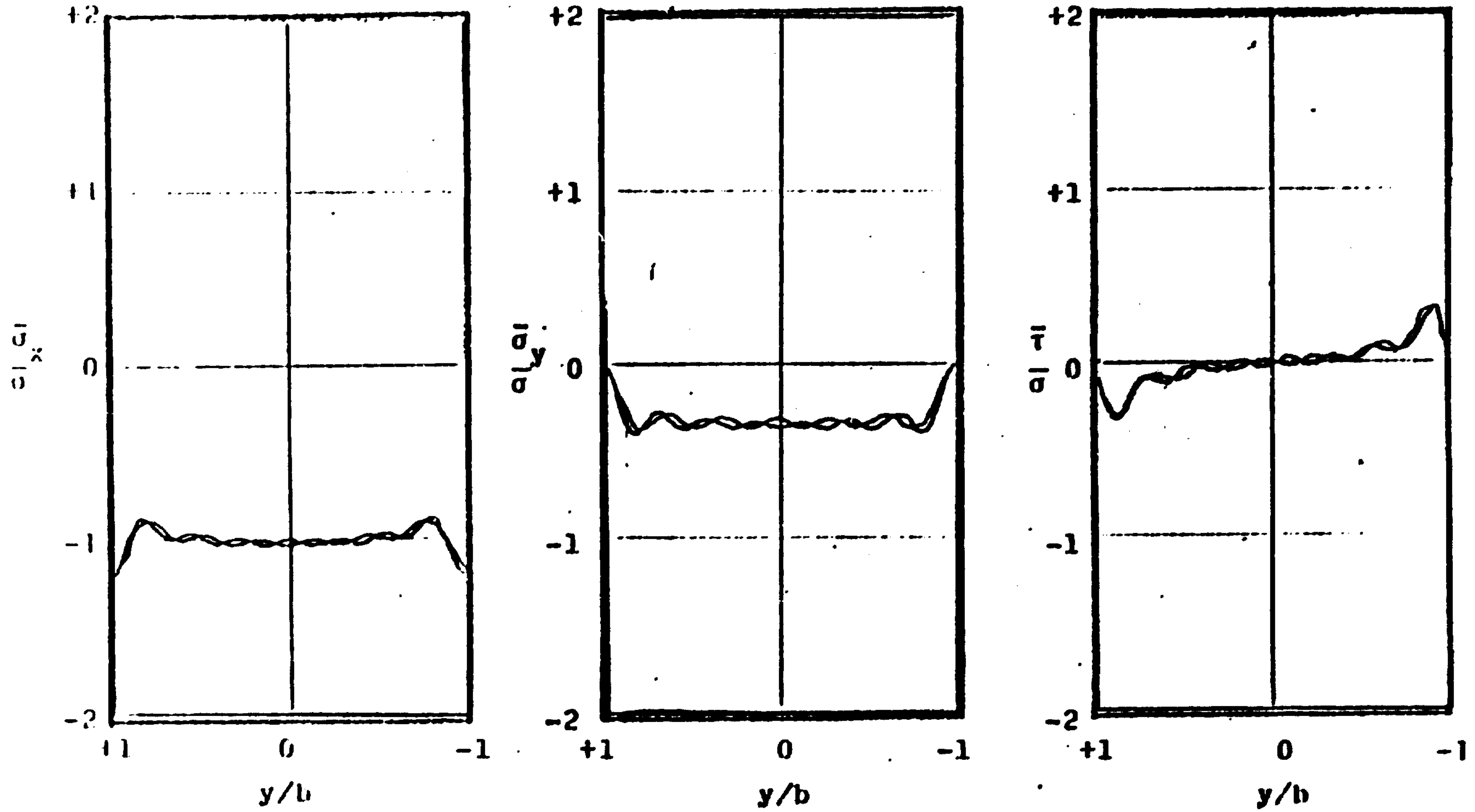

Figure 9 Compression, Q-I laminate, ξ=1/4, x/L=1, N=6,7

STRESS DISTRIBUTION DIAGRAM

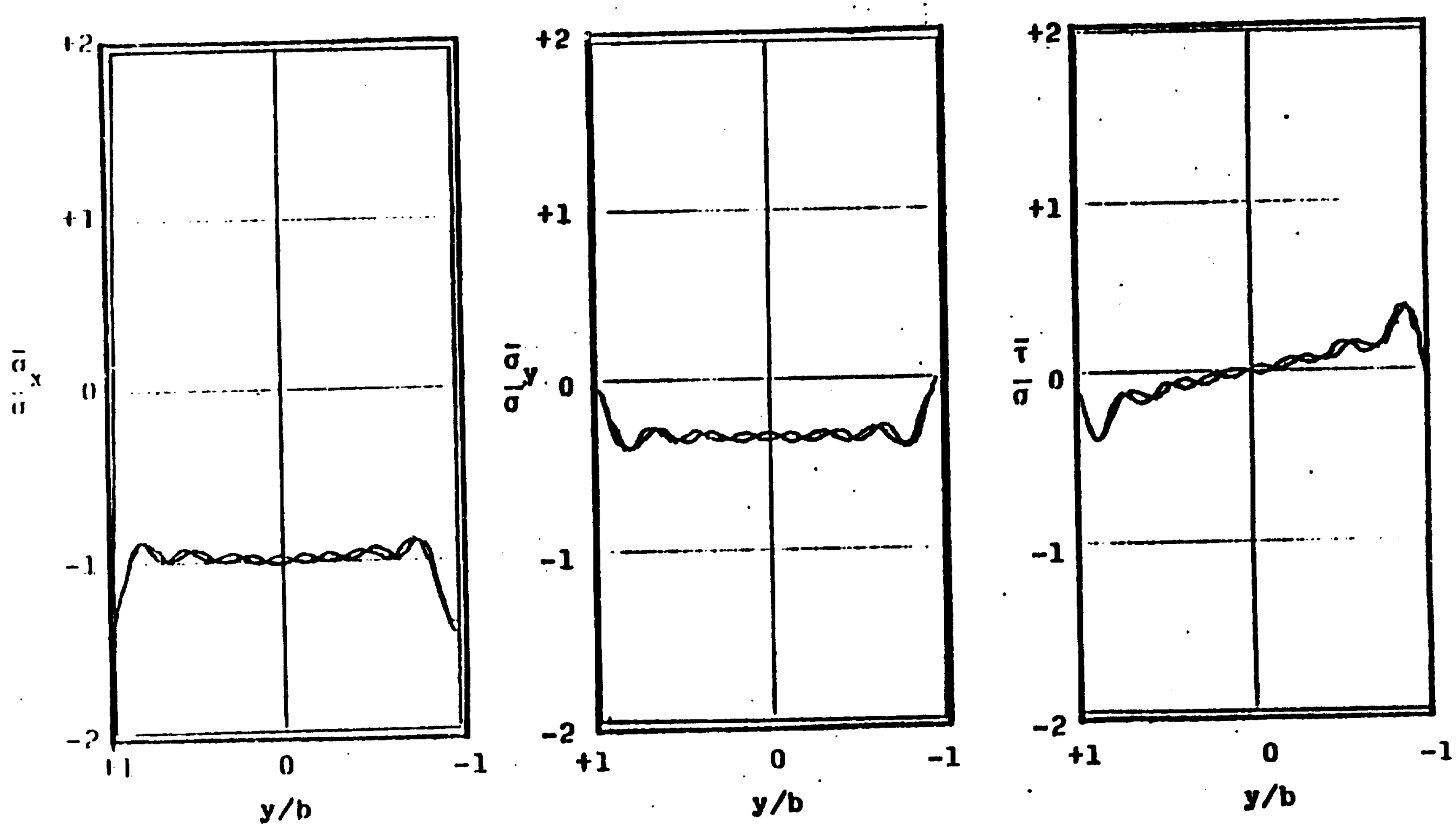

Figure 10 Compression, 0-I laminate, ξ=1/2, x/L=1, N=6,7

STRESS DISTRIBUTION DIAGRAM

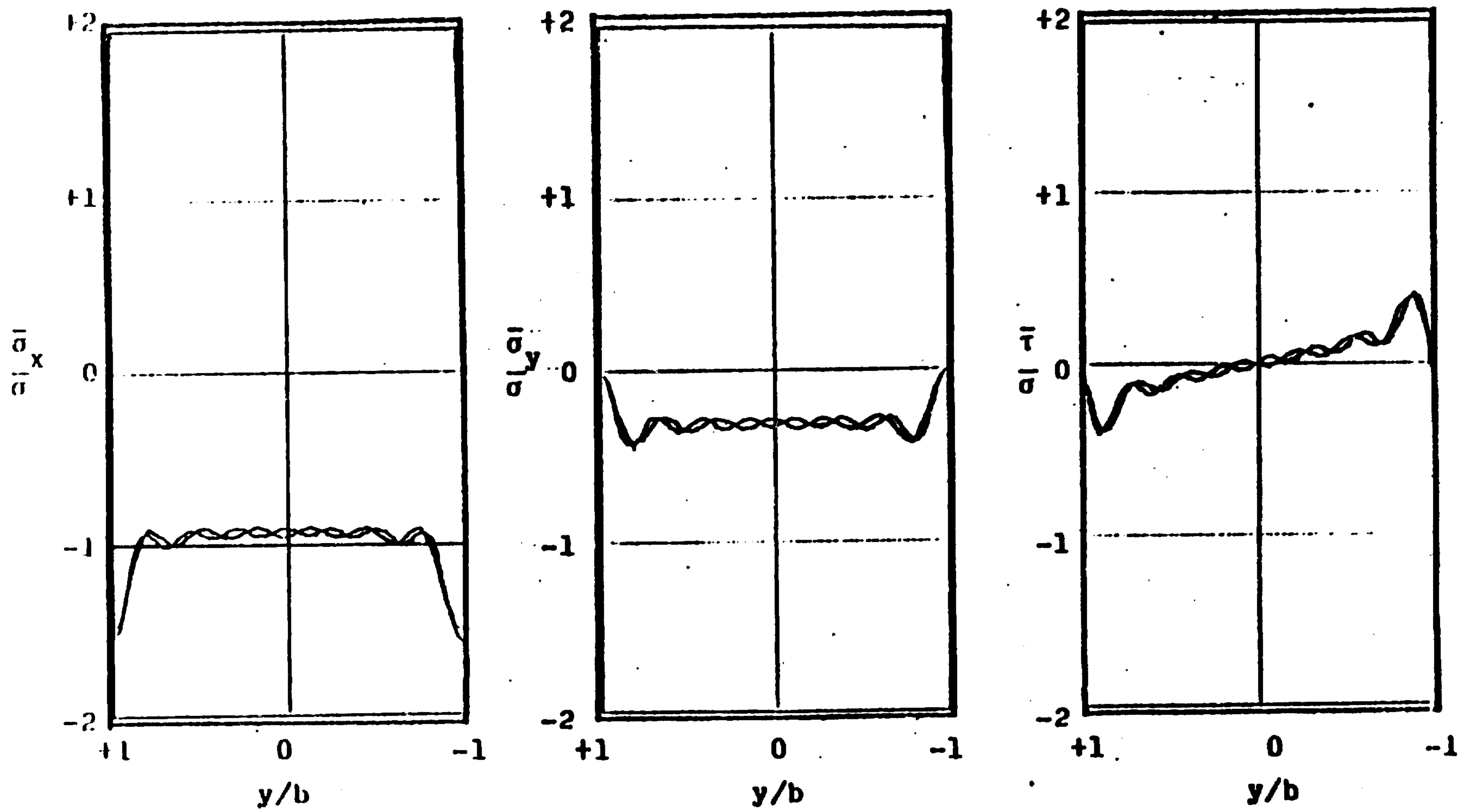

Figure 11 Compression, Q-I laminate, $\xi=1$, $x/L=1$, $N=6,7$

STRESS DISTRIBUTION DIAGRAM

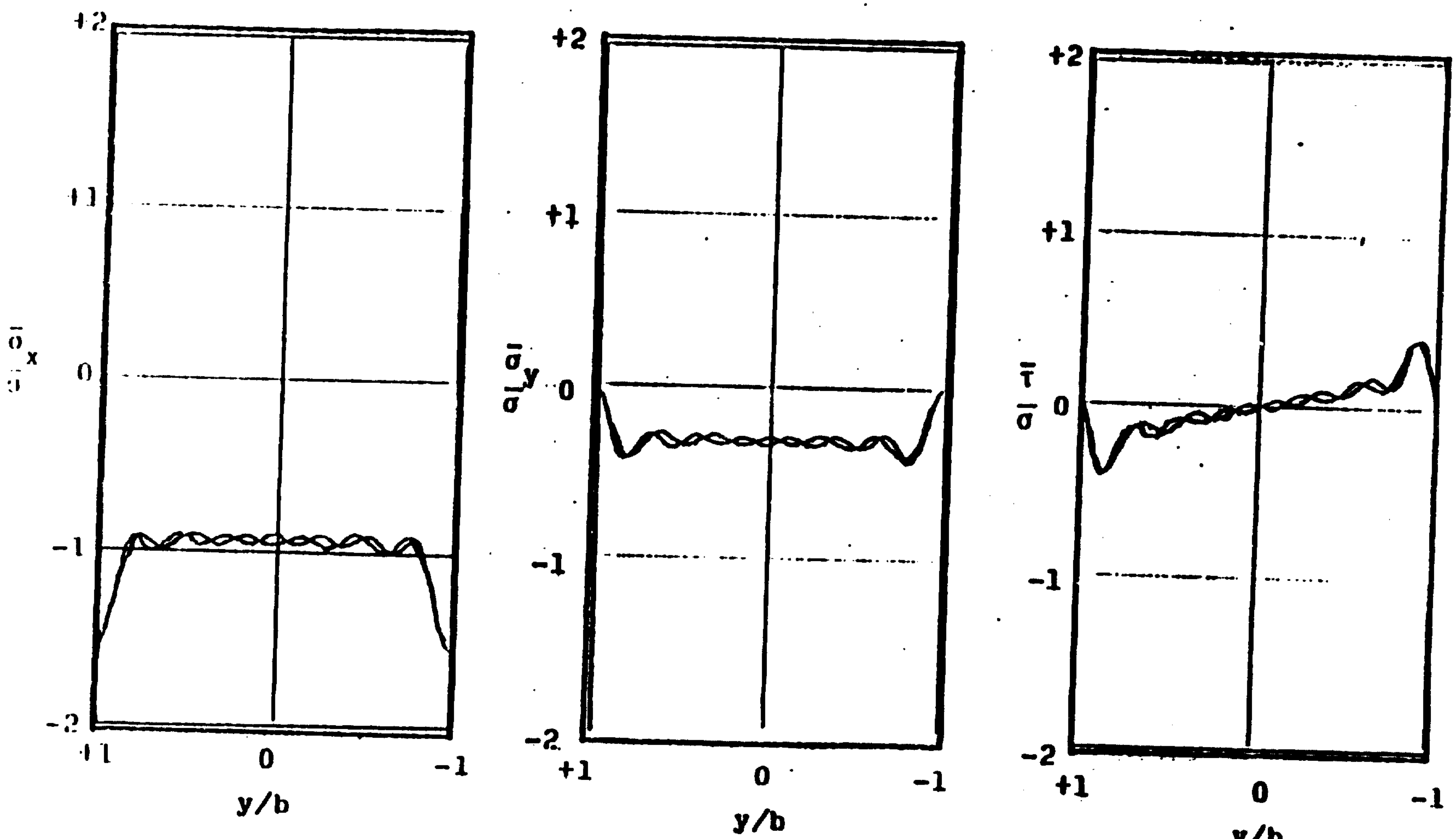

Figure 12 Compression, Q-I laminate, ξ=3, x/L=1, N=6,7

STRESS DISTRIBUTION DIAGRAM

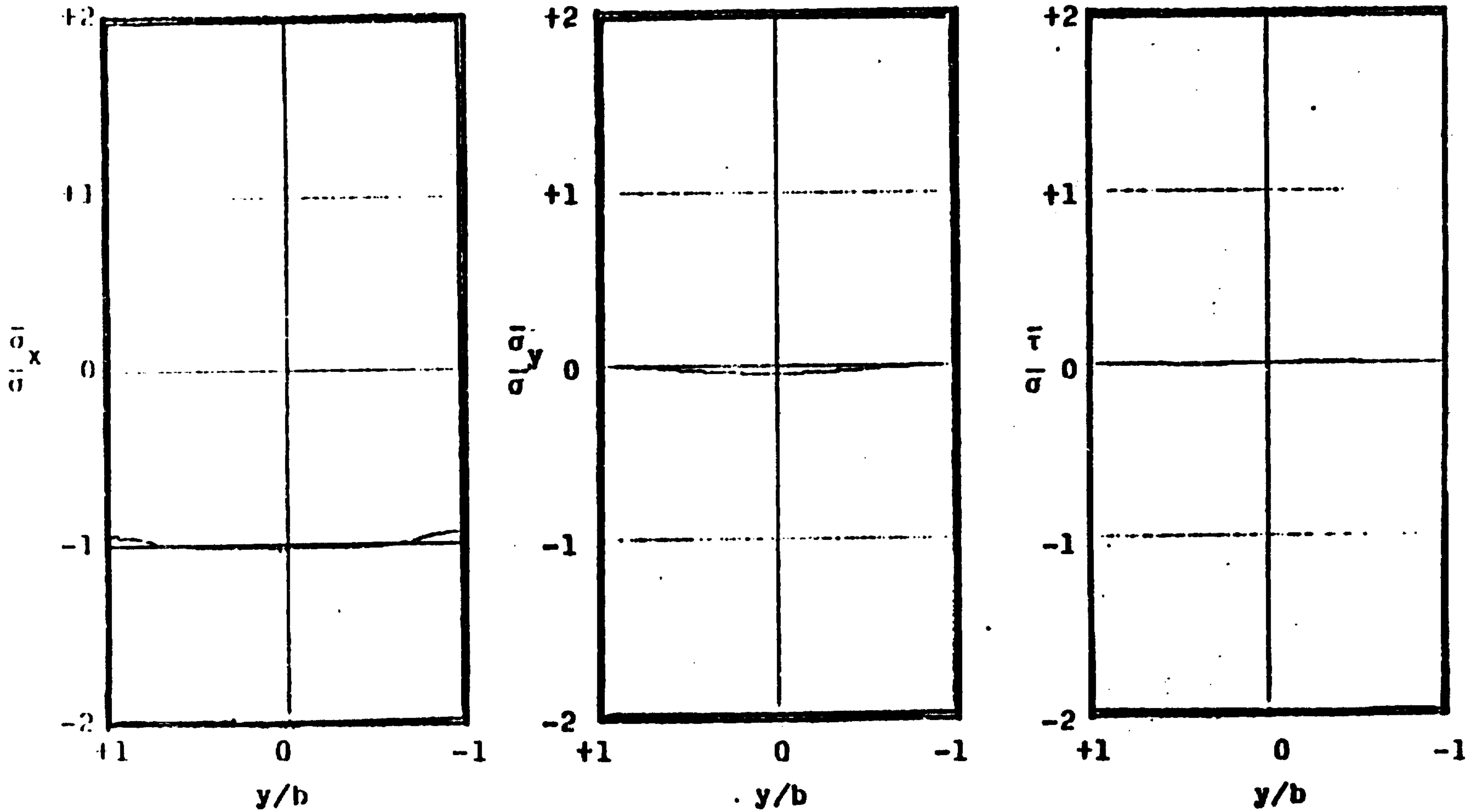

Figure 13 Compression, Q-I laminate, $\xi=6, x/L=0.875$, N=3,4

STRESS DISTRIBUTION DIAGRAM

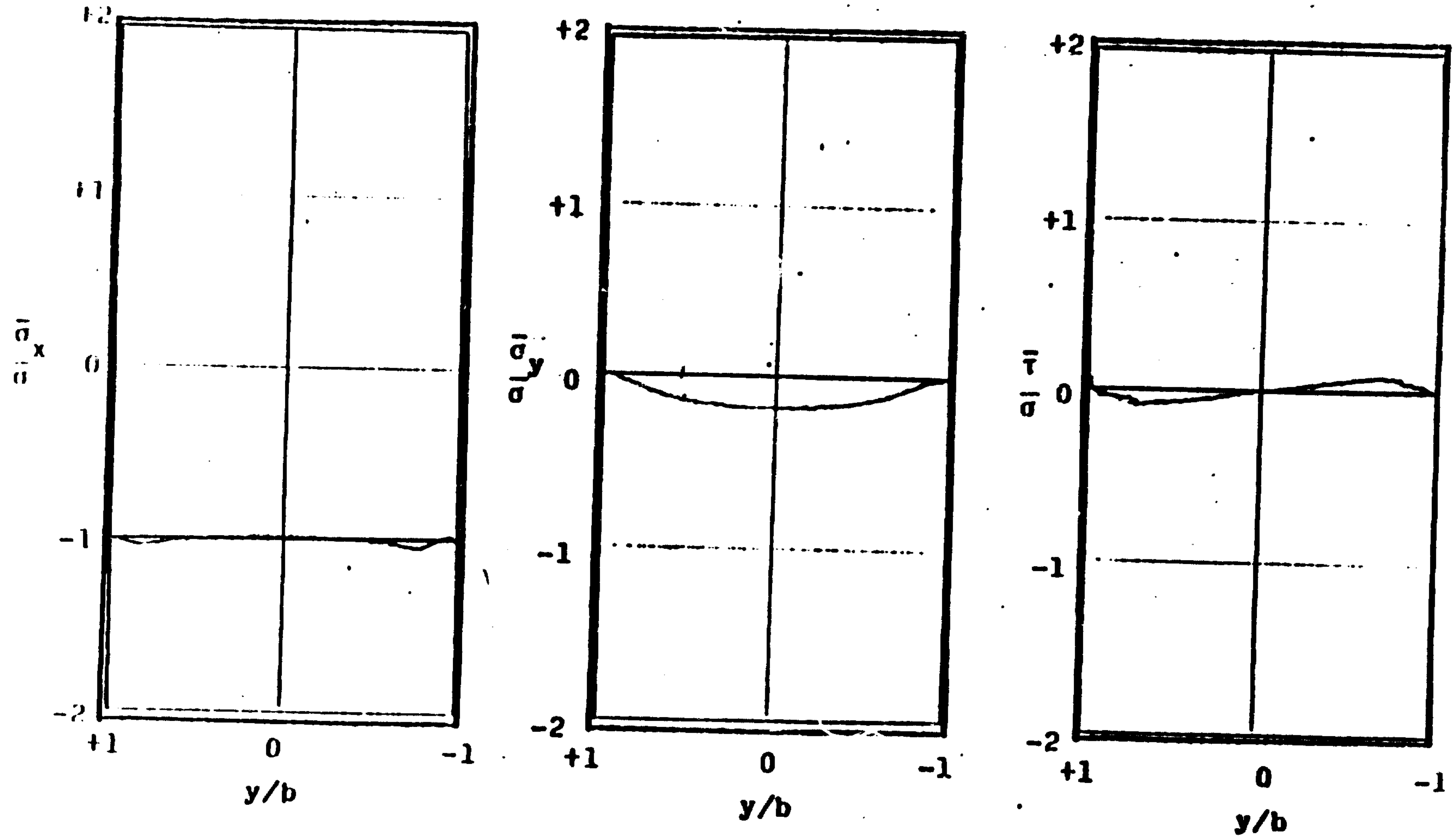

Figure 14 Compression, O-I laminate, ξ=6, x/L=0.95, N=6,7

STRESS DISTRIBUTION DIAGRAM

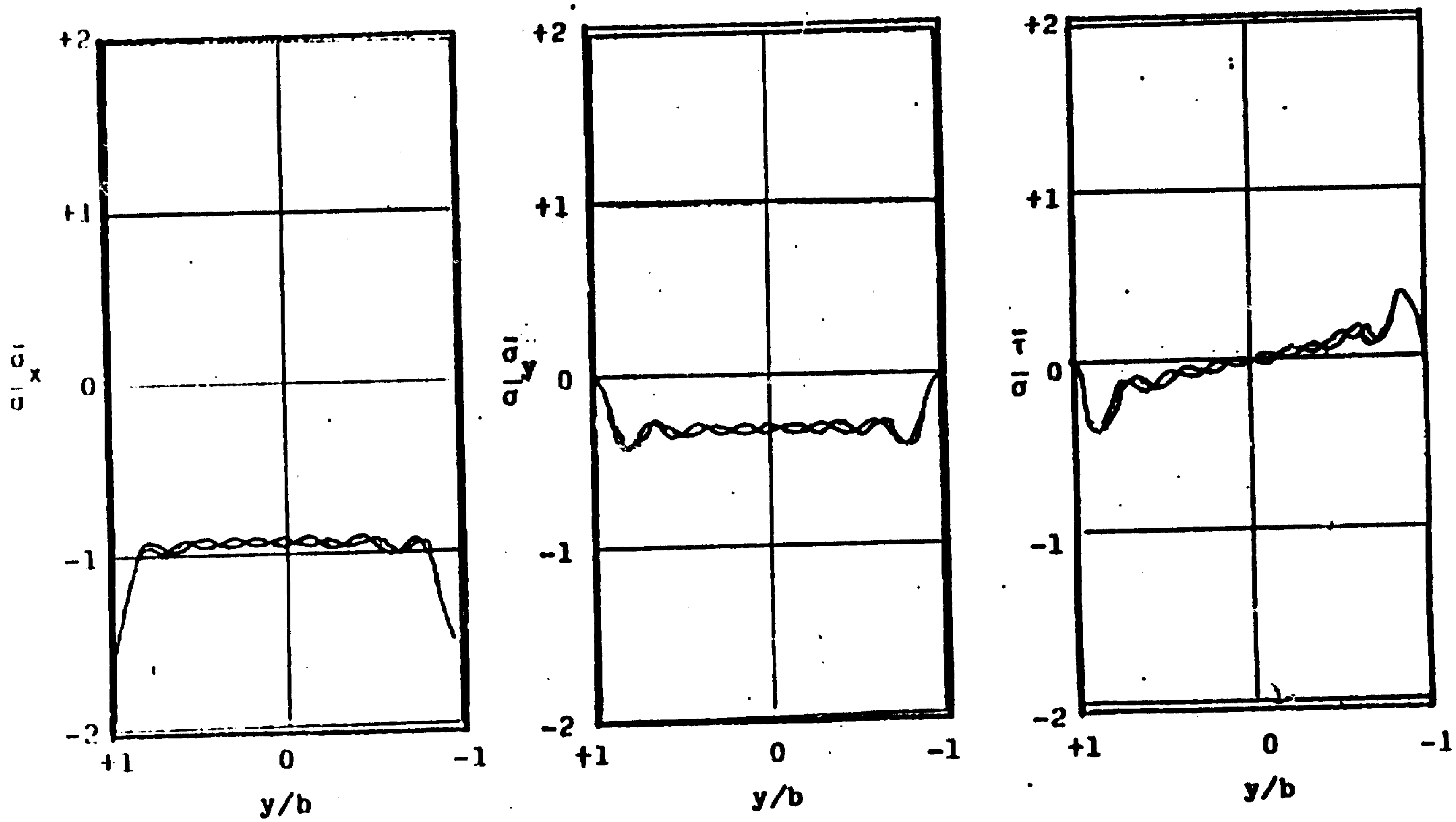

Figure 15 Compression, Q-I laminate, ξ=6, x/L=1, N=6,7

STRESS DISTRIBUTION DIAGRAM

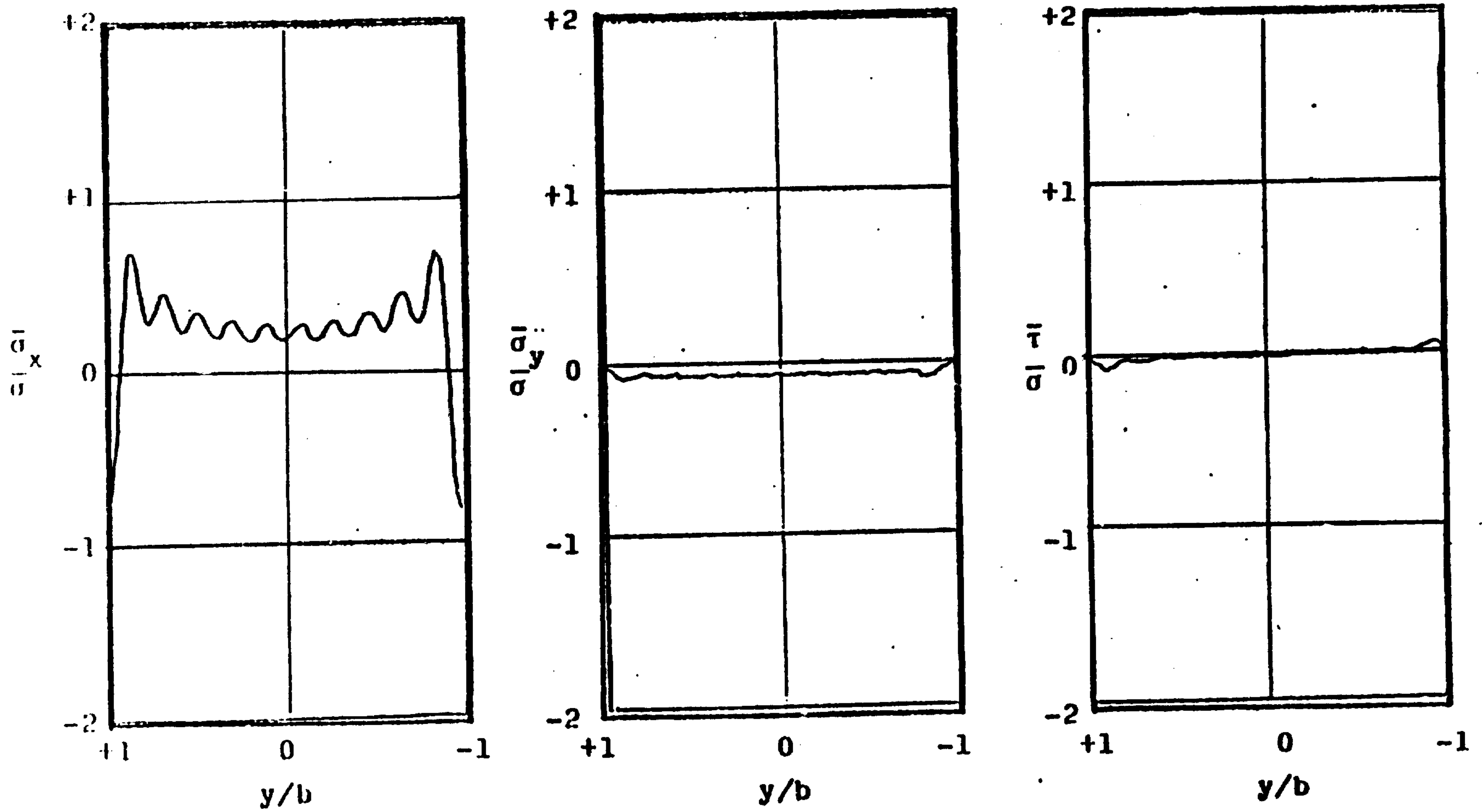

Figure 16 Compression, Q-I lamina-0°, $\xi=1/4$, x/L=1, N=10

STRESS DISTRIBUTION DIAGRAM

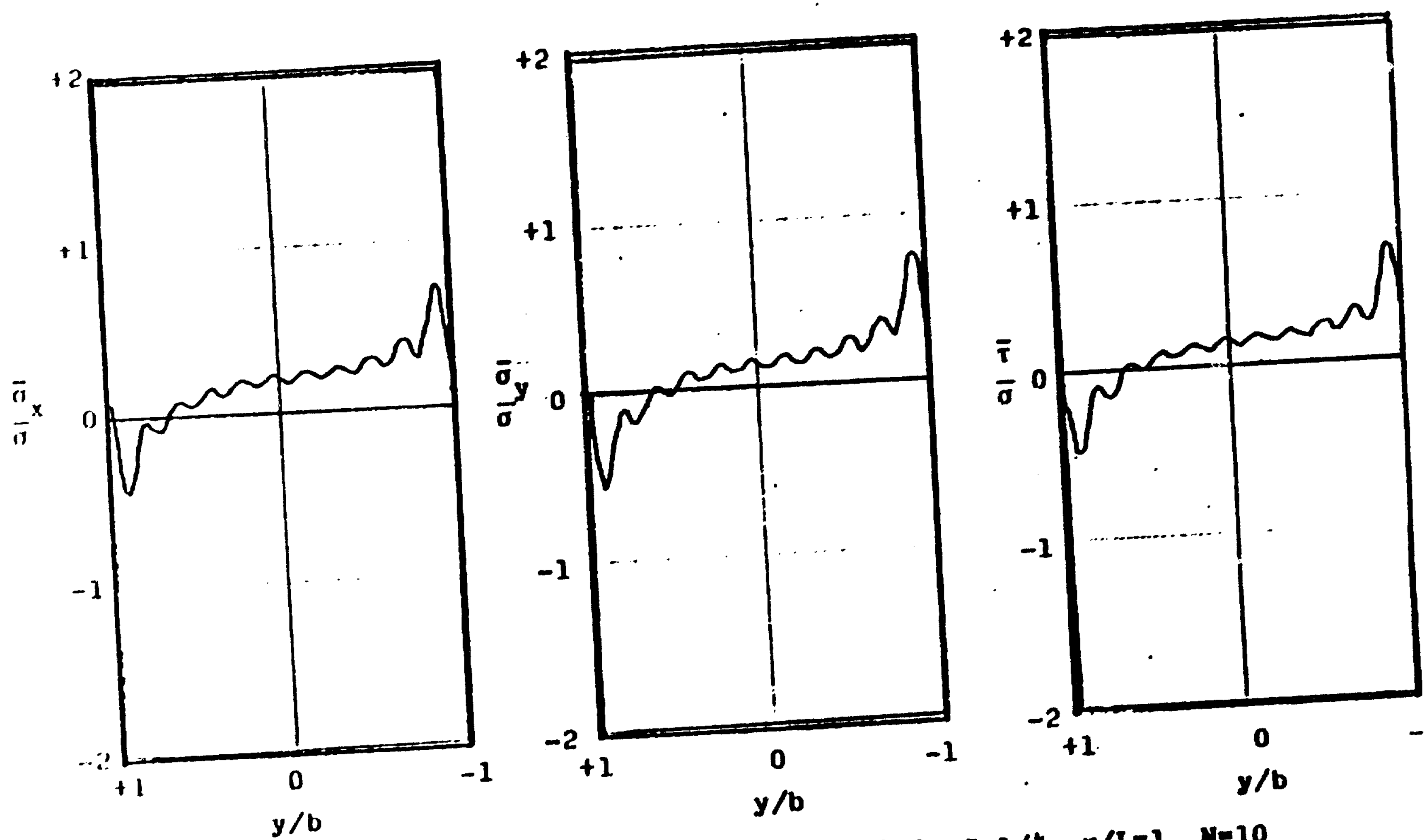

Figure 17 Compression, Q-I lamina-45°, $\xi=1/4$, $x/L=1$, $N=10$

STRESS DISTRIBUTION DIAGRAM

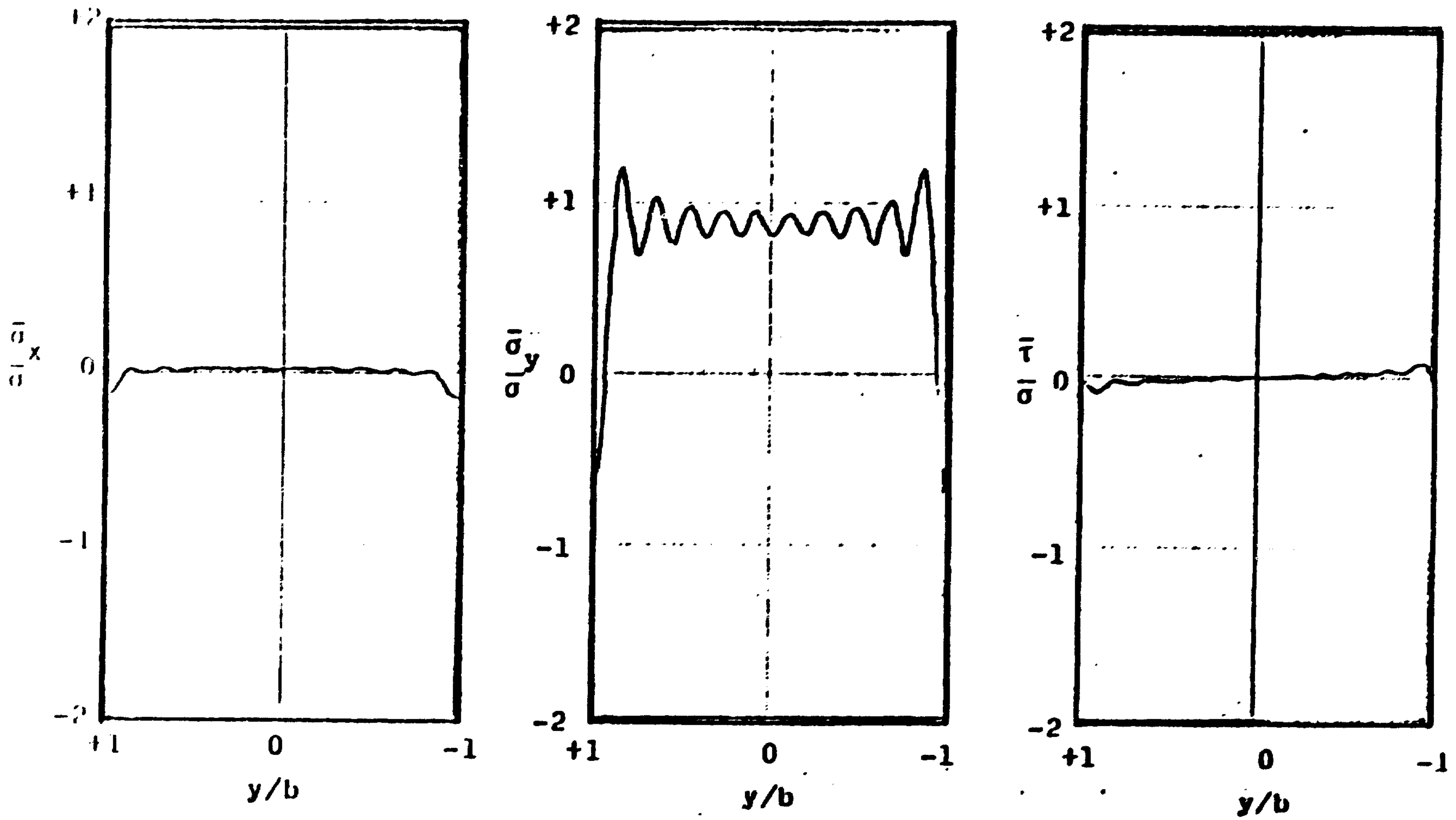

Figure 18 Compression, Q-I lamina-90°, $\xi=1/4$, $x/L=1$, $N=10$

oriented at $\theta=0°$, $45°$, $90°$ respectively. The particular plots are for $\xi=1/4$.

b. Cross-Ply (C-P) $[\pm 45]_s$ Laminates

1. Generalized Plane Stress

Unlike Q-I laminates, C-P laminates have a negative material constant $\Gamma_o=-1.77$*, and a relatively large value for Poisson's ratio ($\nu=0.801$*). As a result of the high value of ν, the influence of the constrained edge should be expected to be much greater than for Q-I laminates.

Just like for Q-I laminates, the eigenvalues are again complex. [See Table 4]. Convergence was somewhat slower than for Q-I laminates; more terms were needed to obtain a reasonable approximation to the stress distributions at the edges. Figures 19 and 20 show the stress distributions at x=L, for $\xi=1/4$ and $\xi=3$, respectively, for N=9 and 10. However, for the region $x/L<0.9$, a 6 term approximation showed excellent convergence. For example, see Fig. 21 for which $\xi=3$; stresses at $x/L=0.9$ are plotted for N=6 and N=7.

* This value was obtained for:

$E_1=21\times10^3$ ksi , $E_2=1.7\times10^3$ ksi , $\nu_{12}=0.21$,
$G_{12}=0.65\times10^3$ ksi , $E=7.95\times10^3$ ksi

TABLE 4, Eigenvalues for C-P laminate in pure compression

N \ α		1	2	3	4	5	6	7	8	9	10
1	Re	0.44	0.44	0.44	0.44	0.44	0.44	0.44	0.44	0.44	0.44
	Im	0.62	0.62	0.62	0.61	0.61	0.61	0.61	0.61	0.61	0.61
2	Re		0.88	0.89	0.89	0.89	0.89	0.89	0.89	0.89	0.89
	Im		1.53	1.52	1.51	1.51	1.51	1.51	1.51	1.51	1.51
3	Re			1.33	1.33	1.34	1.34	1.34	1.34	1.34	1.34
	Im			2.44	2.42	2.41	2.41	2.40	2.40	2.41	2.40
4	Re				1.78	1.79	1.79	1.79	1.79	1.79	1.79
	Im				3.34	3.32	3.31	3.30	3.30	3.29	3.30
5	Re					2.23	2.23	2.24	2.24	2.24	2.25
	Im					4.24	4.21	4.20	4.20	4.19	4.19
6	Re						2.69	2.69	2.69	2.69	2.70
	Im						5.14	5.11	5.10	5.09	5.09
7	Re							3.14	3.14	3.15	3.15
	Im							6.03	6.01	6.00	5.98
8	Re								3.59	3.59	3.60
	Im								6.93	6.90	6.89
9	Re									4.04	4.05
	Im									7.83	7.80
10	Re										4.50
	Im										8.72

Once again there appears to be a singularity at the corners $x=\pm L$, $y=\pm b$. The data, tabulated in Table 5, certainly do not suggest convergence.

In Table 6, the values of $u^{\circ}E_x/\sigma_c L$ are tabulated for C-P laminates, and the convergence for increasing N is slower. Also, observe that for very small aspect ratios, the apparent stiffness increase is well over 100%.

According to the aforedefined axial stress state [Eq. (32)], the domain influenced by constrained edge turns out to be precisely double that of Q-I laminates. Consequently, an aspect ratio for which $\xi=3$ is the smallest length-width ratio for which Eq. (32) is satisfied along the center line $x=0$. For $\xi>3$, a uniaxial stress field will exist in a region around the center line $x=0$; the range of length 3b, the domain influenced by the constraint has length 3b, measured from the edges $x=\pm L$.

2. Lamina stress

Since the lamina stresses are linear combinations of the averaged stresses $\bar{\sigma}_x$, $\bar{\sigma}_y$, $\bar{\tau}$, [see Eq. (29)], lamina stresses will converge at the same rate as the average stresses. The stresses at the corners at the clamped

TABLE 5. Normalized stress at corners $\sigma_x(L,b)/\sigma_c$ for C-P laminate in pure compression

	$\sigma_x(L,b)/\sigma_c$					
N \ ξ	0.25	0.50	1	3	6	
1	0.61	1.16	1.58	1.48	1.48	
2	0.74	1.21	1.93	1.82	1.82	
3	0.86	1.37	2.20	2.08	2.08	
4	0.93	1.50	2.43	2.31	2.31	
5	1.03	1.62	2.63	2.50	2.50	
6	1.10	1.73	2.82	2.68	2.68	
7	1.16	1.83	2.99	2.84	2.83	
8	1.22	1.92	3.15	2.99	2.99	
9	1.29	2.01	3.30	3.12	3.12	
10	1.34	2.09	3.42	3.26	3.26	

TABLE 6. Values of $u^{\circ}E_x/\sigma_c L$ for C-P laminate in pure compression

$u^{\circ}E_x/\sigma_c L$						
N \ ξ	0.25	0.50	1	3	6	
1	0.4775	0.5488	0.7727	0.9335	0.9668	
3	0.4308	0.5073	0.7205	0.9183	0.9592	
5	0.4232	0.4979	0.7082	0.9147	0.9573	
6	0.4212	0.4956	0.7051	0.9137	0.9569	
7	0.4198	0.4939	0.7029	0.9131	0.9565	

STRESS DISTRIBUTION DIAGRAM

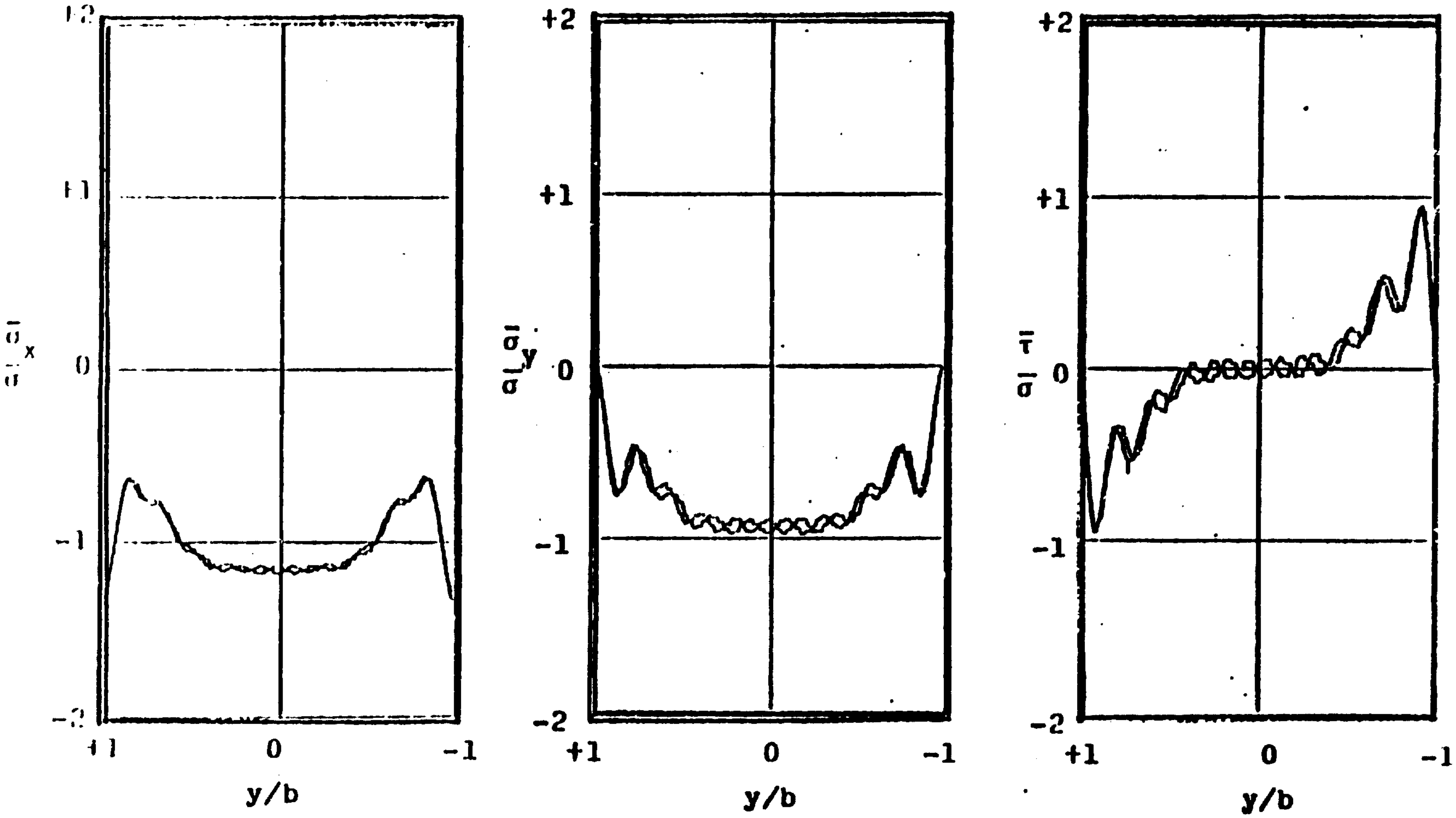

Figure 19 Compression, C-P laminate, $\xi=1/4$, $x/L=1$, $N=9,10$

STRESS DISTRIBUTION DIAGRAM

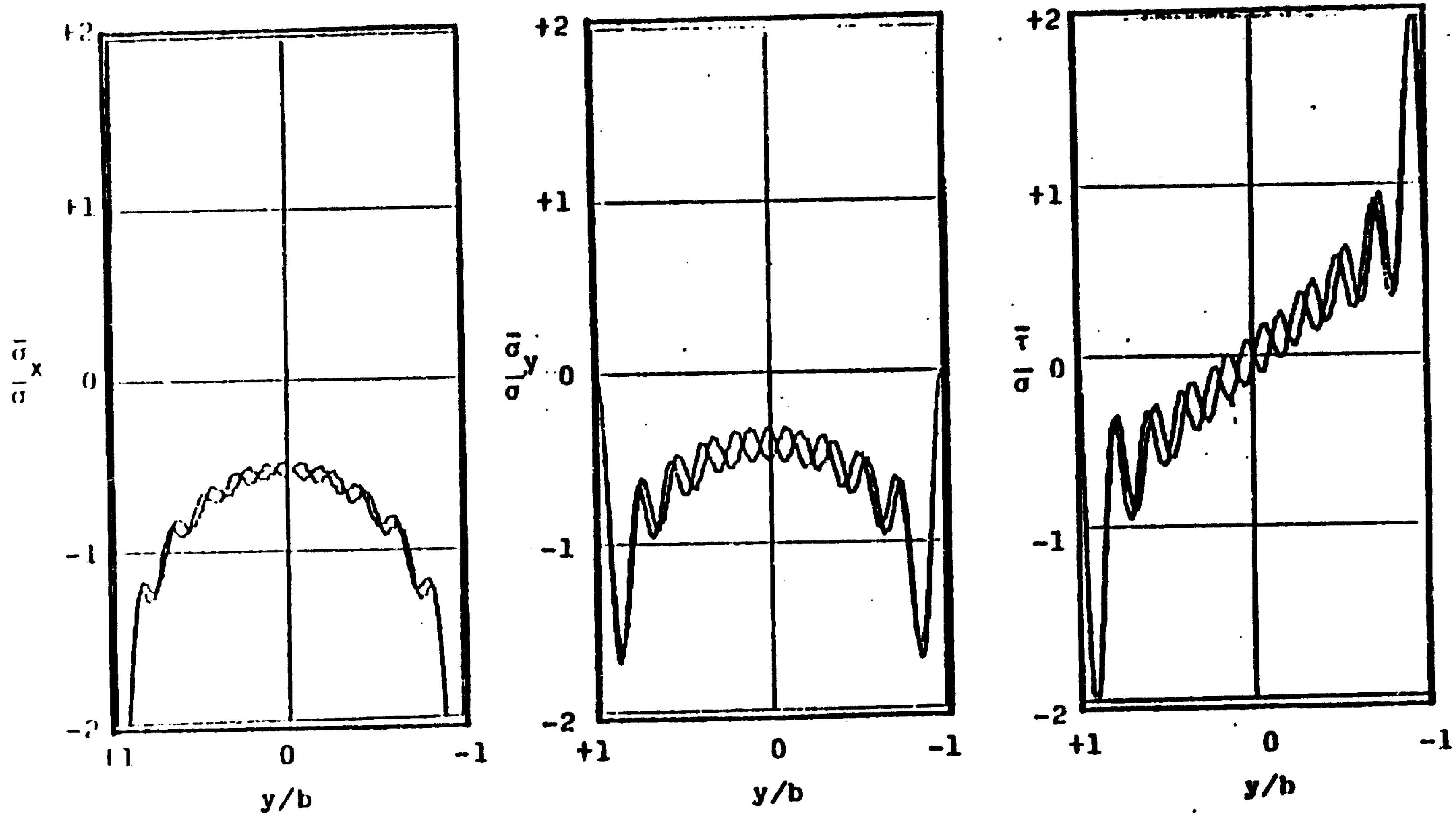

Figure 20 Compression, C-P laminate, $\xi=3$, $x/L=1$, $N=9,10$

STRESS DISTRIBUTION DIAGRAM

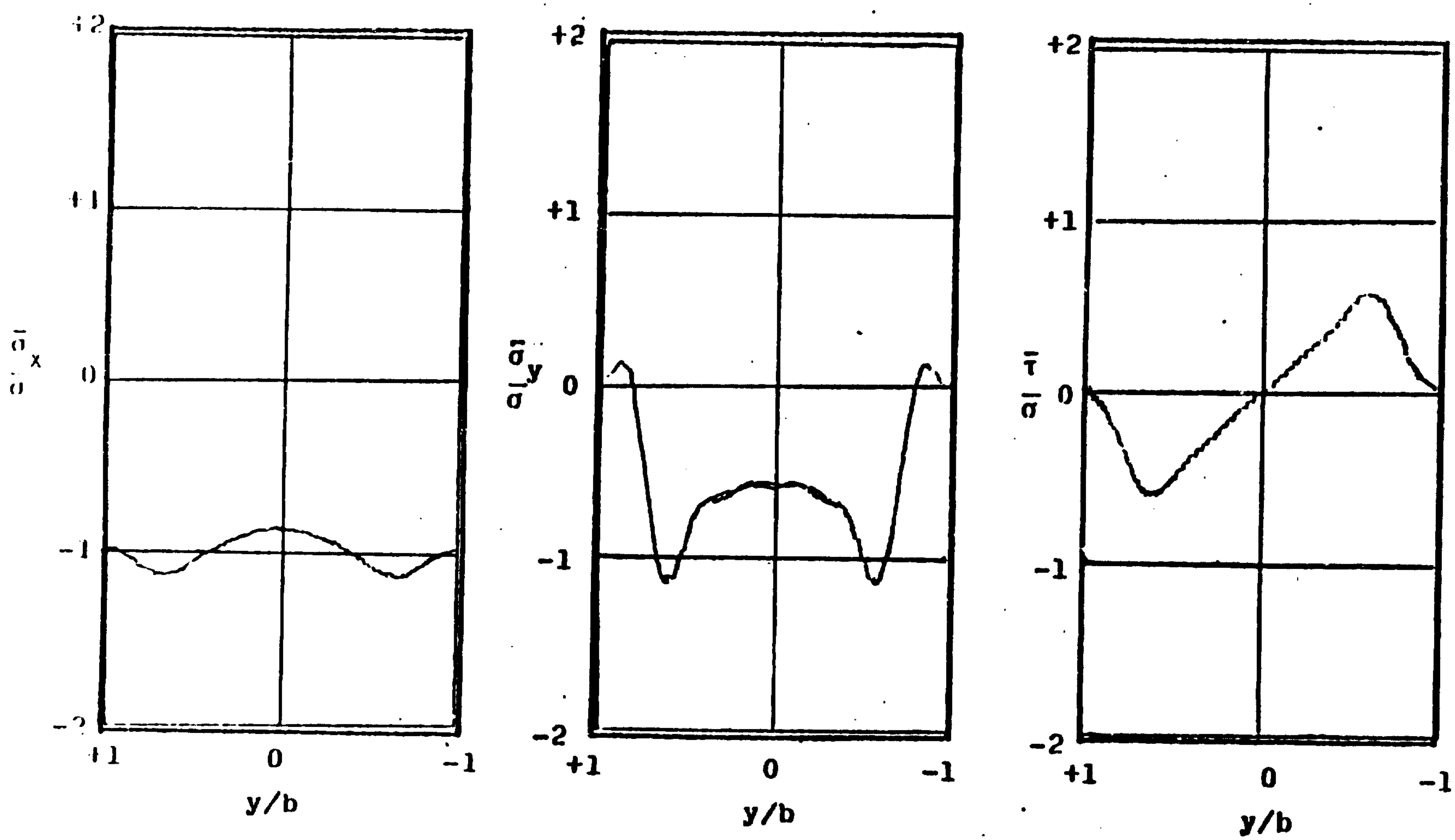

Figure 21 Compression, C-P laminate, $\xi=3$, $x/L=0.9$, $N=9,10$

STRESS DISTRIBUTION DIAGRAM

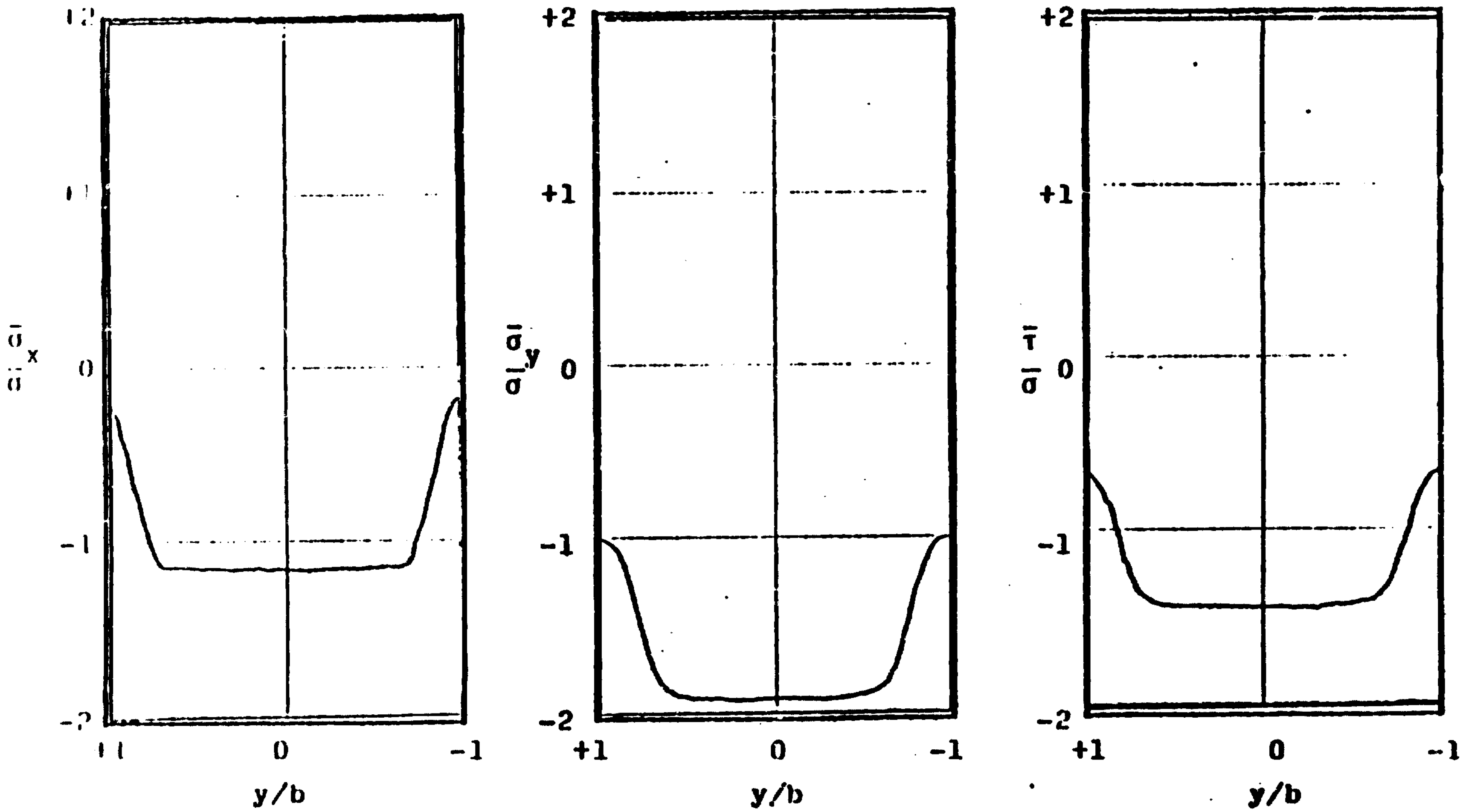

Figure 22 Compression, C-P lamina-45°, $\xi=3$, x/L=0, N=10

edges will exhibit sigularities. However, for the region away from the edges, the stress distributions appear very well behaved. For example, see Fig. (22) in which $\xi=3$, $x=0$ (at the center line), $N=10$, $\theta=45°$.

c. Unidirectional (U-D) $[0]_s$ Laminates

Since all fibers lie in the same direction, the generalized plane stresses and lamina stresses are the same. Also $E_x=E_1$, $E_y=E_2$, $\nu_{xy}=\nu_{12}$ and $G_{xy}=G_{12}$. For the assumed data $G_{12}=0.65x10^3$ ksi, $\nu_{12}=0.21$, we compute $\Gamma_o=2.581$.

Unlike the previous two laminates, the eigenvalues of U-D laminates were real. Table 7 lists the eigenvalues for up to 3 terms. Figure (23) shows the resulting stress distributions at the edge for $\xi=3$. The values of stress $\bar{\sigma}_x$ at the corners for different ξ are tabulated in Table 8 for N ranging from 1 to 3. According to our definition, a uniaxial stress state does exist everywhere except at the corners.

Table 7. Eigenvalues for U-D laminate in pure compression

N	1	2	3
I-1	0.181	0.181	0.181
I-2		0.362	0.362
I-3			0.547
II-1	0.910	0.846	0.809
II-2		2.620	2.539
II-3			4.272

STRESS DISTRIBUTION DIAGRAM

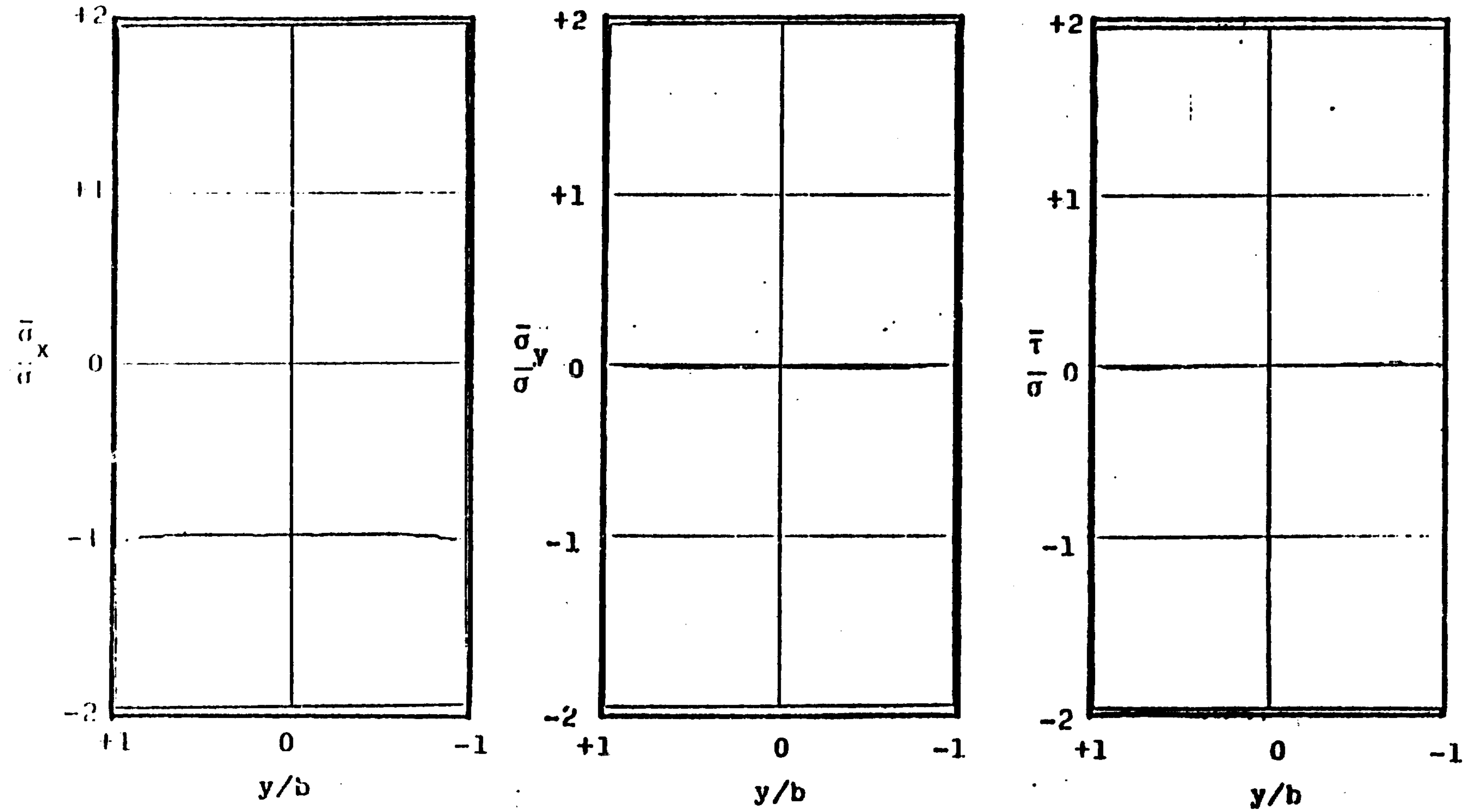

Figure 23 Compression, U-D laminate, $\xi=1$, $x/L=1$, N=2,3

TABLE 8. Normalized stress at corners $\bar{\sigma}_x(L,b)/\sigma_c$ for U-D laminate in pure compression

$\bar{\sigma}_x(L,b)/\sigma_c$						
N \ ξ	0.25	0.50	1	3	6	
1	1.000	1.004	1.008	1.010	1.011	
2	1.002	1.009	1.016	1.020	1.020	
3	1.005	1.014	1.023	1.028	1.028	

B. Pure Bending

Convergence of the solution in bending was faster than for pure compression for both the Q-I and C-P laminates. This suggested that the Legendre polynomial may be preferable to a Fourier series for similar mixed boundary value problems. Since the axial stress $\bar{\sigma}_x$, when reduced to elementary bending stress, is linear in y, it is apparent that Fourier series will take many terms to approximate $\bar{\sigma}_x$ in y-coordinate while the first order Legendre polynomial is equal to y.

a. Quasi-Isotropic

1. Generalized Plane Stress

Eigenvalues are shown in Table 9 for N ranging from 1 to 8. Observe that the eigenvalues are increasing at a faster rate with the number of terms for $N \geq 5$ than the corresponding case in pure compression [see Table 1]. This may account for the apparent faster convergence of these stresses. Fewer terms for approximation of the stresses are needed than for pure compression [compare $\bar{\sigma}_x$ in Figs.12 and 24].

The effect of the constrained edge is comparable to the pure compression case. Outside of the region of

TABLE 9. Eigenvalues for Q-I laminate in pure bending

$n \backslash \alpha$		1	2	3	4	5	6	7	8		
1	Re	3.66	3.74	3.75	3.75	3.75	3.75	3.75	3.75		
	Im	1.54	1.38	1.38	1.38	1.38	1.38	1.38	1.38		
2	Re		6.84	6.87	6.95	6.95	6.95	6.95	6.95		
	Im		2.63	1.74	1.67	1.68	1.68	1.68	1.68		
3	Re			10.50	9.94	10.10	10.10	10.10	10.10		
	Im			4.35	2.32	1.88	1.86	1.86	1.86		
4	Re				14.80	13.20	13.10	13.30	13.30		
	Im				6.58	3.29	2.22	2.00	2.00		
5	Re					19.80	16.90	16.30	16.30		
	Im					9.23	4.59	2.85	2.20		
6	Re						25.60	21.10	19.70		
	Im						12.30	6.11	3.75		
7	Re							32.10	25.70		
	Im							15.80	7.82		
8	Re								39.30		
	Im								19.60		

STRESS DISTRIBUTION DIAGRAM

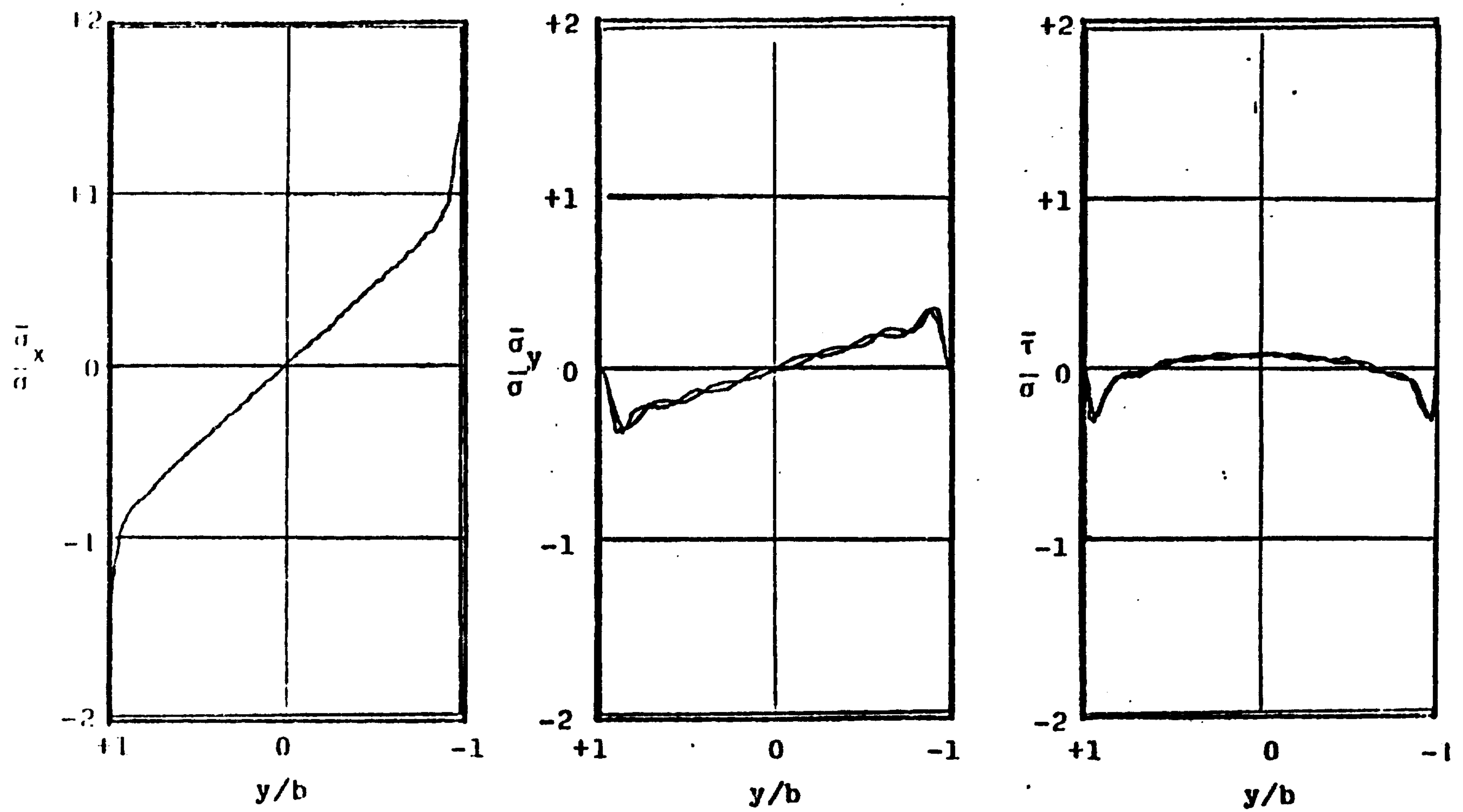

Figure 24 Bending , Q-I laminate, $\xi = 3$, $x/L = 1$, $N = 5, 6$

influence of the constrained edge, the axial stress is linear and the other stresses vanish [Fig.25] exactly as predicted by elementary theory.

Another measure of the constrained edge effect is provided by Table 10, in which values for $\theta^\circ 2b^2/3M_b S_{11}\xi$ are tabulated for various ξ and N. Again, note that as N increases, the value θ°/M_b rapidly converges. Also as ξ increases, the value $\theta^\circ 2b^2/3M_b S_{11}\xi$ tends toward unity, the predicted value from Bernoulli-Euler deflection theory.

A possible stress singularity at the corners, $x=\pm L$, $y=\pm b$, is very much in evidence from the stress plots in Fig. 24. Alternatively, the value of $\bar{\sigma}_x(L,b)$ is tabulated for different N in Table 11. and shows no sign of converging.

2. Lamina Stress

Figures 26-28 show the laminae stresses at the constrained edge for the plies oriented at $\theta^\circ=0^\circ$, 45°, 90°, respectively. It is interesting to observe from Fig. 28 that the greatest normal stress occurs in the direction of the fibers (i.e. the y-direction). However, in the 0° lamina (Fig. 26) the greatest stress, except for the corners, occurs transverse to the fibers

TABLE 10. Values of $\theta^{\circ}\cdot 2b^2/3M_bS_{11}\xi$ for Q-I laminate in pure bending

	$\theta^{\circ}\cdot 2b^2/3M_bS_{11}\xi$					
N \ ξ	0.25	0.50	1	3	6	
1	0.965	0.982	0.991	0.997	0.999	
2	0.955	0.976	0.989	0.996	0.998	
4	0.949	0.974	0.987	0.996	0.998	
7	0.948	0.973	0.987	0.996	0.998	
8	0.948	0.973	0.987	0.996	0.998	

TABLE 11. Normalized stress at corners $\sigma_x(L,b)/\sigma_b$ for Q-I laminate in pure bending

$\bar{\sigma}_x(L,b)/\sigma_b$						
N \ ξ	0.25	0.50	1	3	6	
1	1.01	1.08	1.10	1.10	1.10	
2	1.12	1.21	1.22	1.22	1.22	
3	1.25	1.33	1.34	1.34	1.34	
4	1.37	1.45	1.45	1.46	1.46	
5	1.49	1.57	1.57	1.57	1.57	
6	1.58	1.68	1.68	1.68	1.68	
7	1.68	1.79	1.79	1.79	1.79	
8	1.77	1.88	1.89	1.89	1.89	

STRESS DISTRIBUTION DIAGRAM

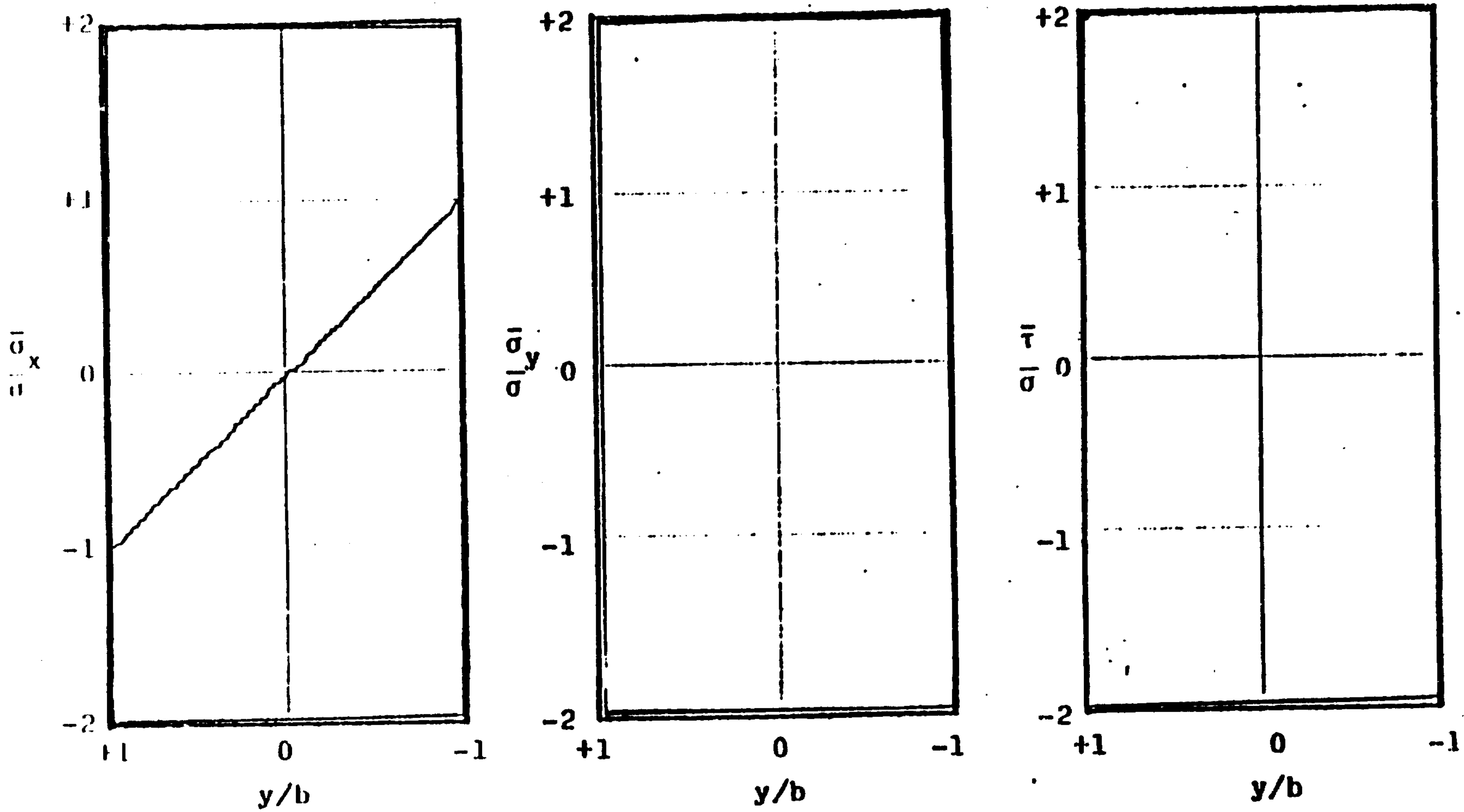

Figure 25 Bending , Q-I laminate, ξ=6, x/L=0.5, N=5,6

STRESS DISTRIBUTION DIAGRAM

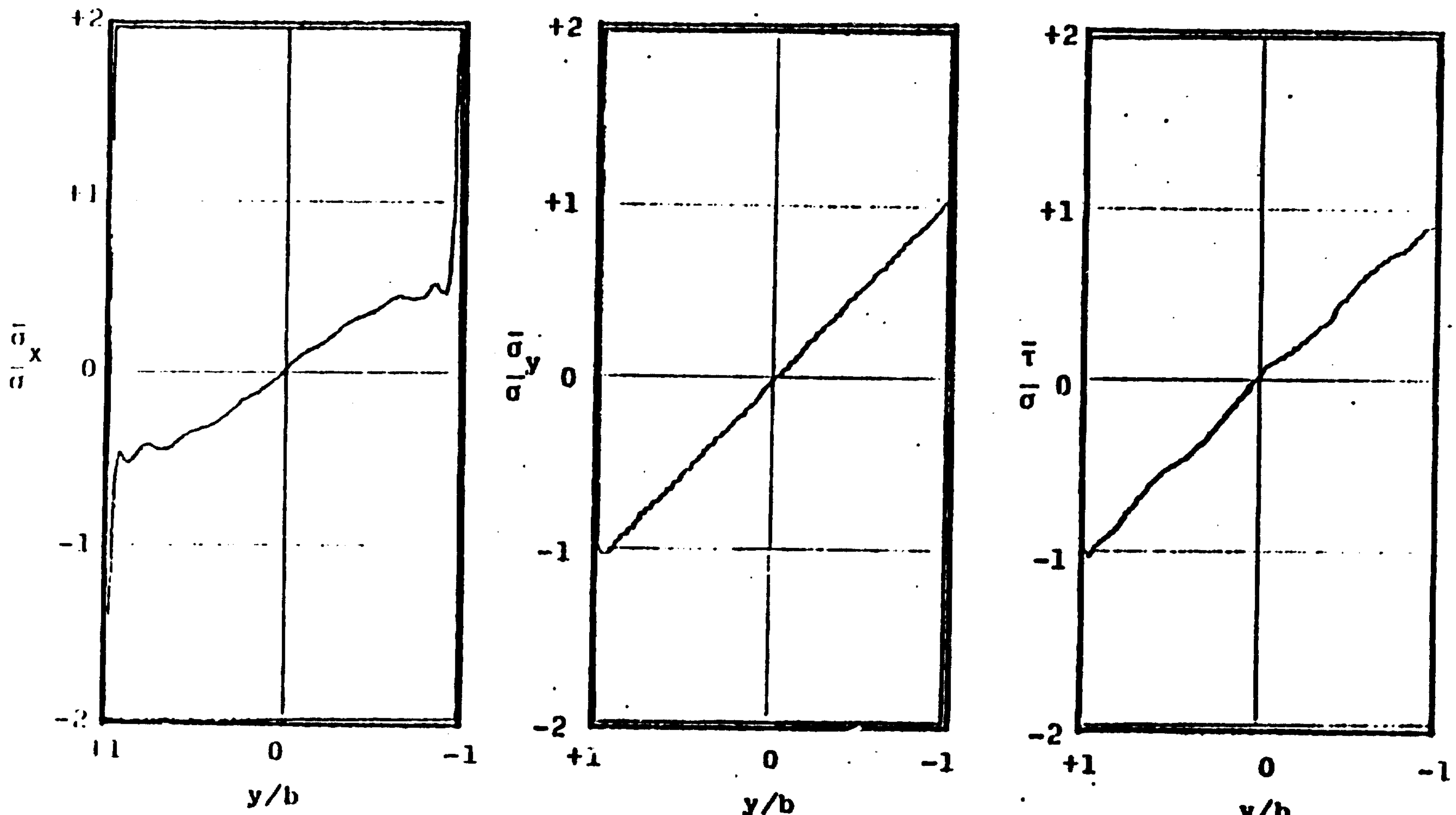

Figure 26 Bending, Q-I lamina-0°, $\xi=1/4$, $x/L=1$, N=8

STRESS DISTRIBUTION DIAGRAM

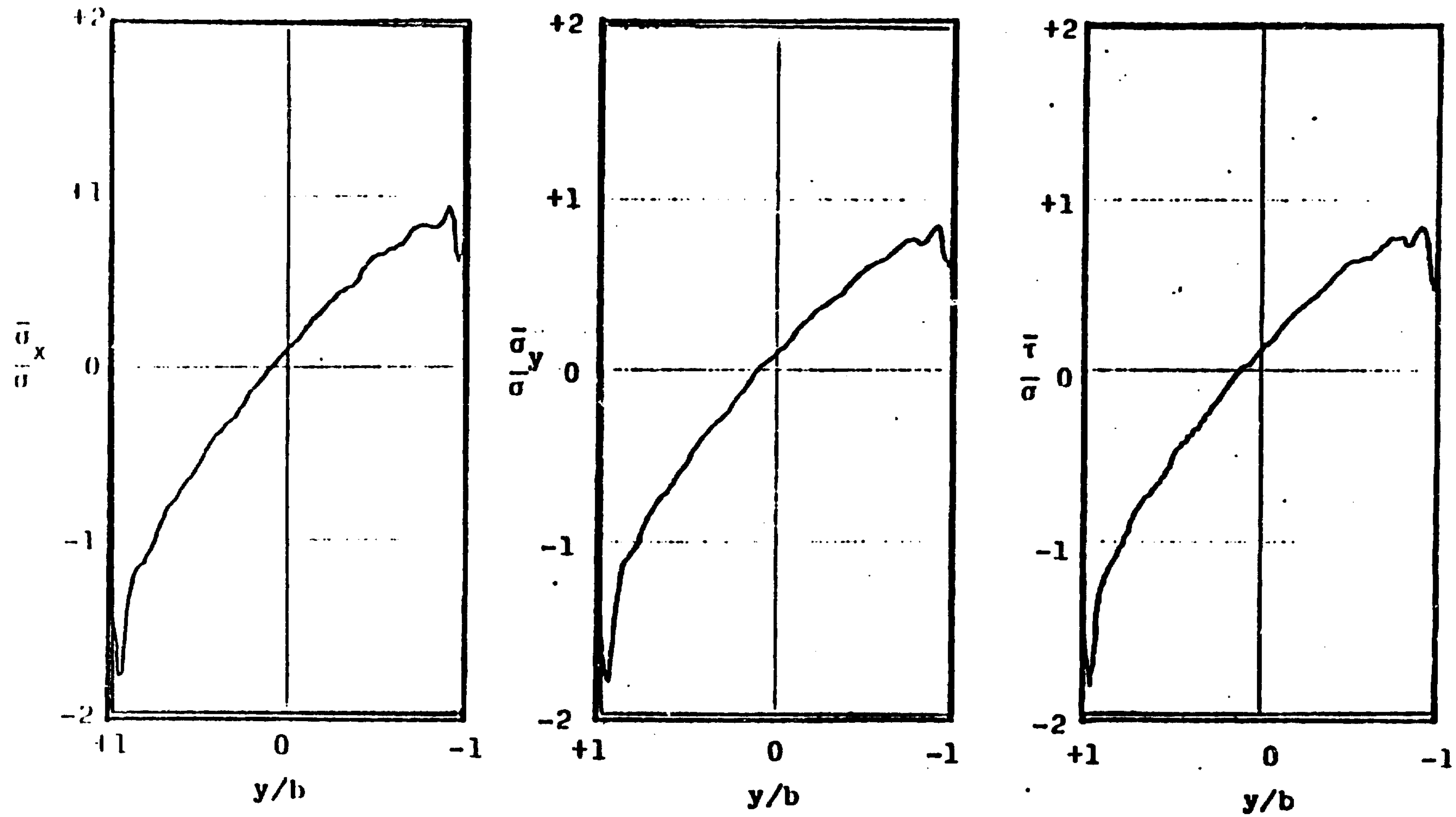

Figure 27 Bending, Q-I lamina-45°, ξ=1/4, x/L=1, N=8

STRESS DISTRIBUTION DIAGRAM

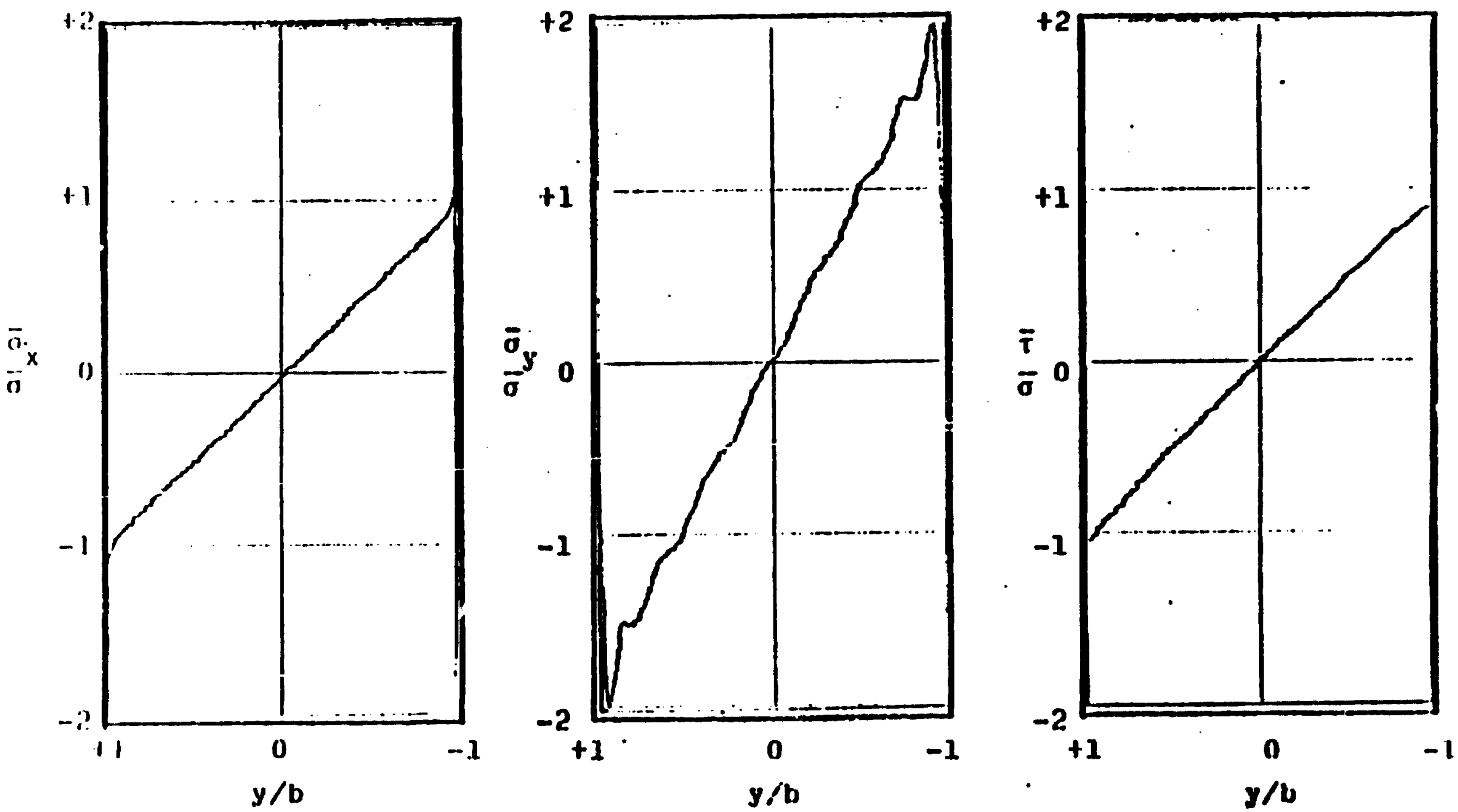

Figure 28 Bending, Q-I lamina-90°, $\xi=1/4$, $x/L=1$, N=8

(also the y-direction).

b. Cross-Ply Laminates

1. Generalized Plane Stress

The eigenvalues for pure bending were once again complex valued and are tabulated in Table 12. The accelerating rate of increase of the eigenvalues is apparent from the Table, and is reflected in the rate of convergence of the stresses [see Fig. 29].

Table 13 provides values for $\theta^{\circ}2b^2/3M_bS_{11}\xi$ and is the counterpart to Table 10 for Q-I laminates. As we observed for pure compression, the effect of the constrained edge upon apparent bending stiffness is considerably greater for C-P laminate than Q-I laminate in pure bending also.

Again, evidence of a singular stress state at the corners of the clamped edges is provided by Fig.29. Tabluated values of $\bar{\sigma}_x(\pm L, \pm b)$, as shown in Table 14., also appear to grow without bound for large N.

2. Lamina Stress

Figures 30,31 show representative data for the lamina stress distributions within the C-P laminate.

TABLE 12. Eigenvalues for C-P laminate in pure bending

N \ α		1	2	3	4	5	6	7	8		
1	Re	2.15	2.08	2.08	2.08	2.08	2.08	2.08	2.08		
	Im	3.33	3.35	3.35	3.35	3.35	3.35	3.35	3.35		
2	Re		3.96	3.53	3.51	3.51	3.51	3.51	3.51		
	Im		6.28	6.15	6.15	6.15	6.15	6.15	6.15		
3	Re			6.83	5.09	4.94	4.93	4.93	4.93		
	Im			9.65	9.01	8.95	8.95	8.95	8.95		
4	Re				9.01	6.86	6.43	6.36	6.36		
	Im				13.60	12.07	11.80	11.80	11.80		
5	Re					12.30	8.90	8.02	7.81		
	Im					18.30	15.40	14.70	14.60		
6	Re						16.10	11.20	9.77		
	Im						23.60	19.20	17.80		
7	Re							20.40	13.80		
	Im							29.60	23.40		
8	Re								25.10		
	Im								36.30		

TABLE 13. Value of $\theta^{\circ}\cdot 2b^2/3M_bS_{11}\xi$ for C-P laminate in pure bending

$\theta^{\circ}\cdot 2b^2/3M_bS_{11}\xi$						
N \ ξ	0.25	0.50	1	3	6	
1	0.624	0.786	0.918	0.972	0.986	
2	0.563	0.744	0.897	0.965	0.982	
4	0.539	0.718	0.883	0.960	0.980	
7	0.529	0.708	0.878	0.959	0.979	
8	0.527	0.706	0.877	0.958	0.979	

TABLE 14. Normalized stress at corners $\sigma_x(L,b)/\sigma_c$ for C-P laminate in pure bending

$\bar{\sigma}_x(L,b)/\sigma_b$						
$N \backslash \xi$	0.25	0.50	1	3	6	
1	0.76	1.42	1.37	1.38	1.38	
2	1.26	1.72	1.75	1.76	1.76	
3	1.52	2.09	2.12	2.12	2.12	
4	1.68	2.44	2.48	2.48	2.48	
5	1.97	2.78	2.84	2.83	2.83	
6	2.21	3.12	3.18	3.18	3.18	
7	2.43	3.45	3.52	3.52	3.52	
8	2.67	3.78	3.86	3.85	3.85	

STRESS DISTRIBUTION DIAGRAM

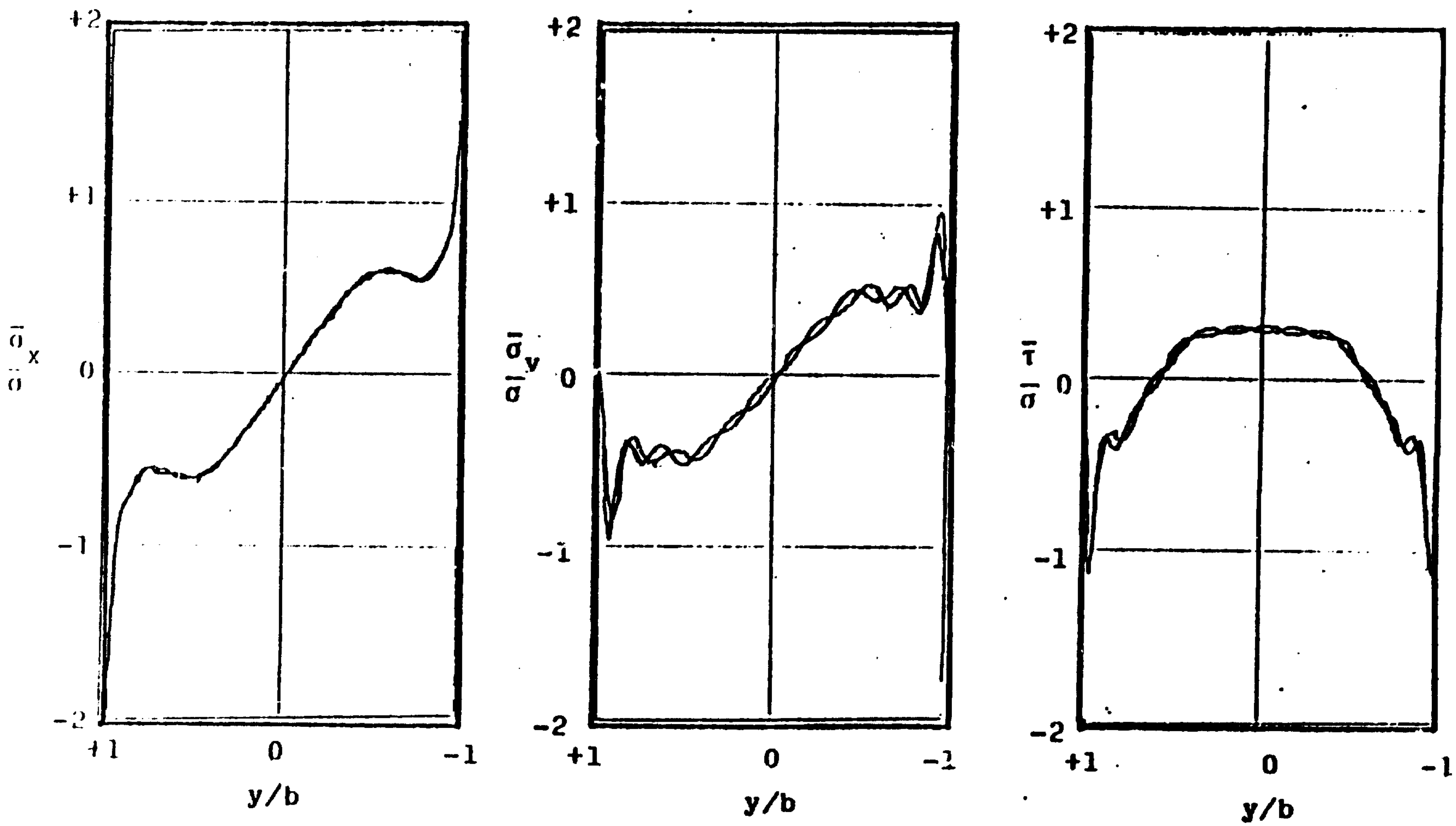

Figure 29 Bending, C-P laminate, $\xi=1/4$, $x/L=1$, $N=7,8$

STRESS DISTRIBUTION DIAGRAM

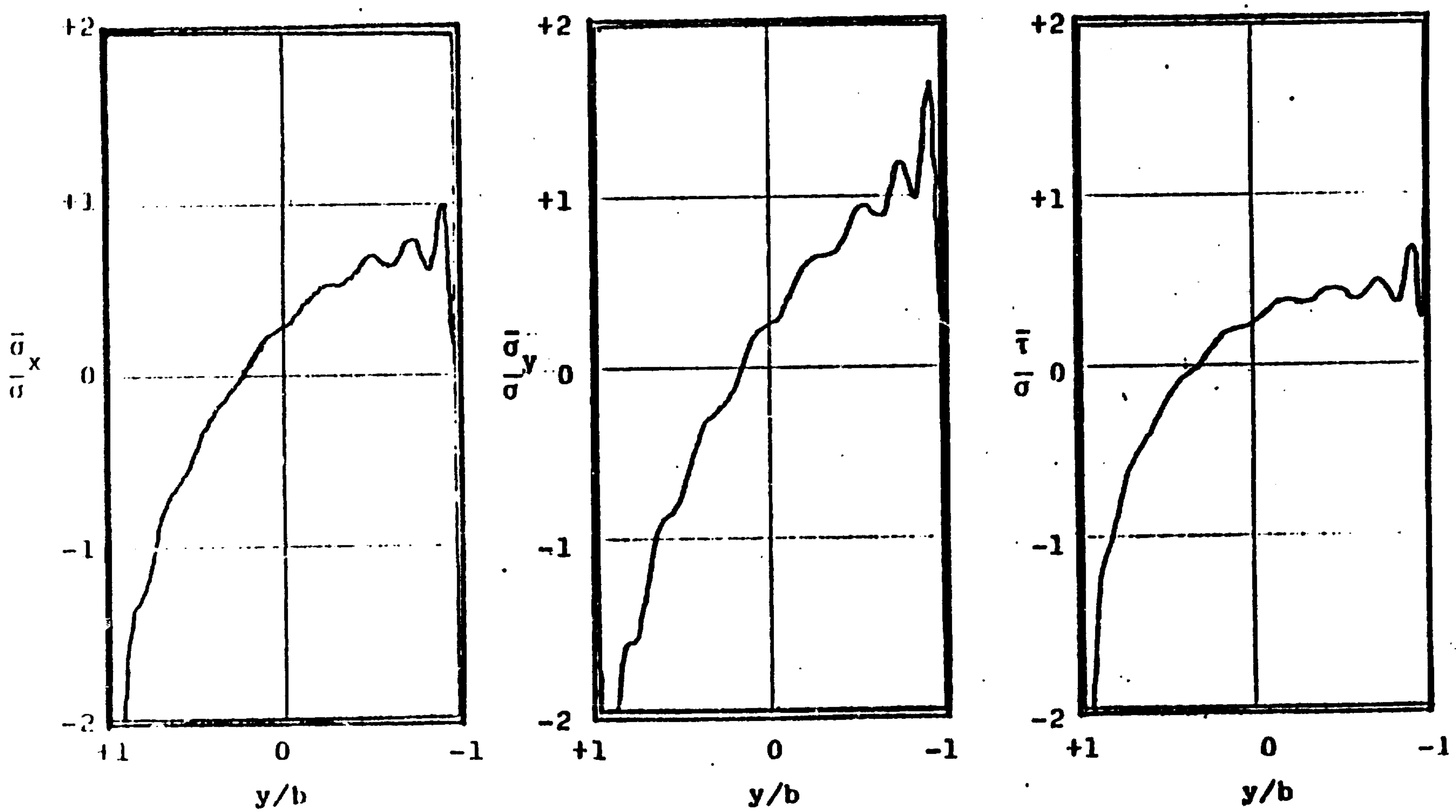

Figure 30 Bending, C-P lamina-45°, ξ=1/4,x/L=1, N=8

STRESS DISTRIBUTION DIAGRAM

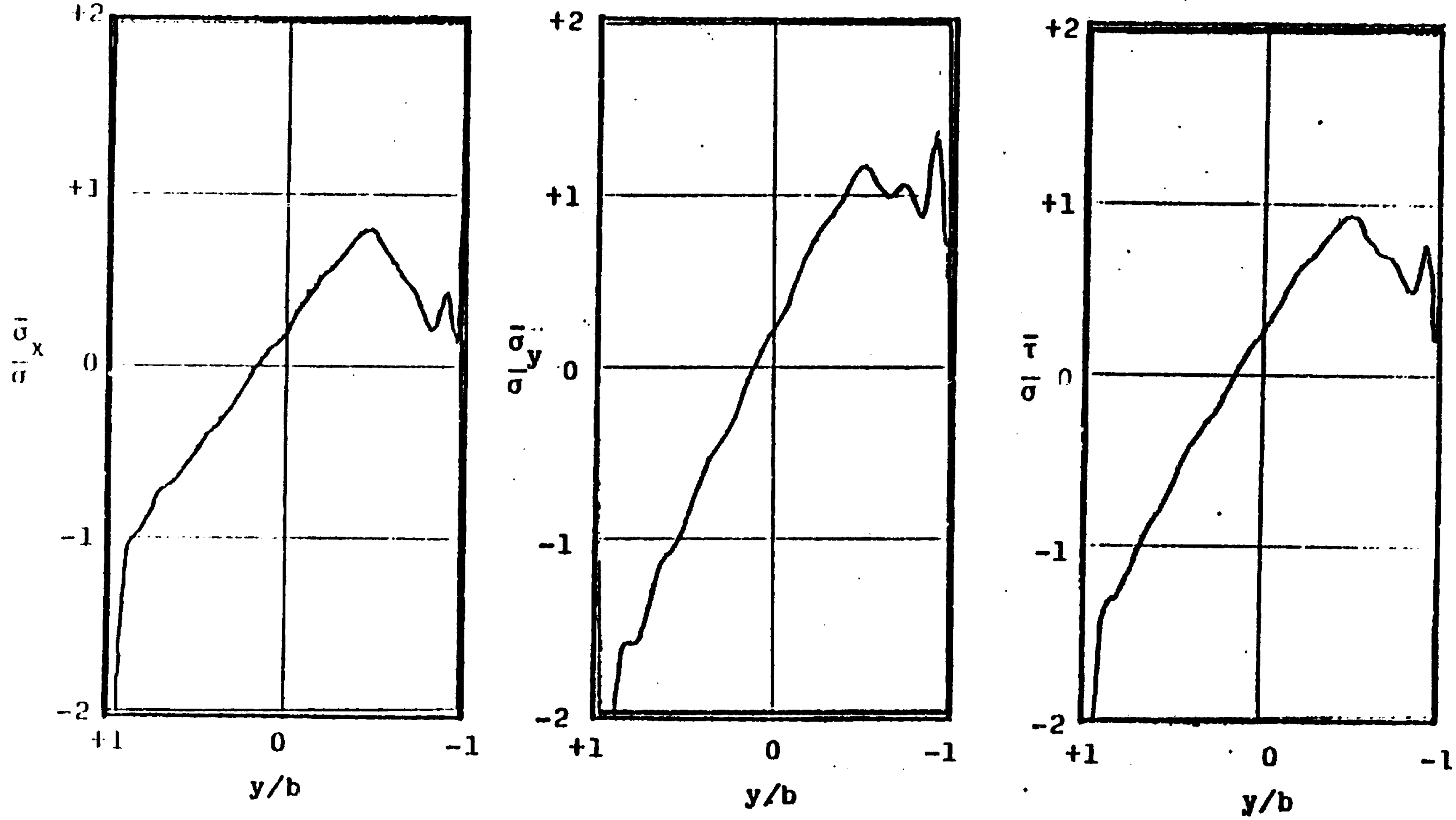

Figure 31 Bending, C-P lamina-45°, $\xi=3$, $x/L=1$, $N=8$

c. Unidirectional (U-D) $[0]_3$ Laminates

Figure 32 shows the axial stress is linear and the other stresses vanish, for $\xi=6$, $x=\pm L$. exactly as predicted by elementary theory. Eigenvalues are real and are tabulated in Table 15, for up to three terms. Again, calculations for axial stress at the corners of the clamped edge suggest a possible singularity.

STRESS DISTRIBUTION DIAGRAM

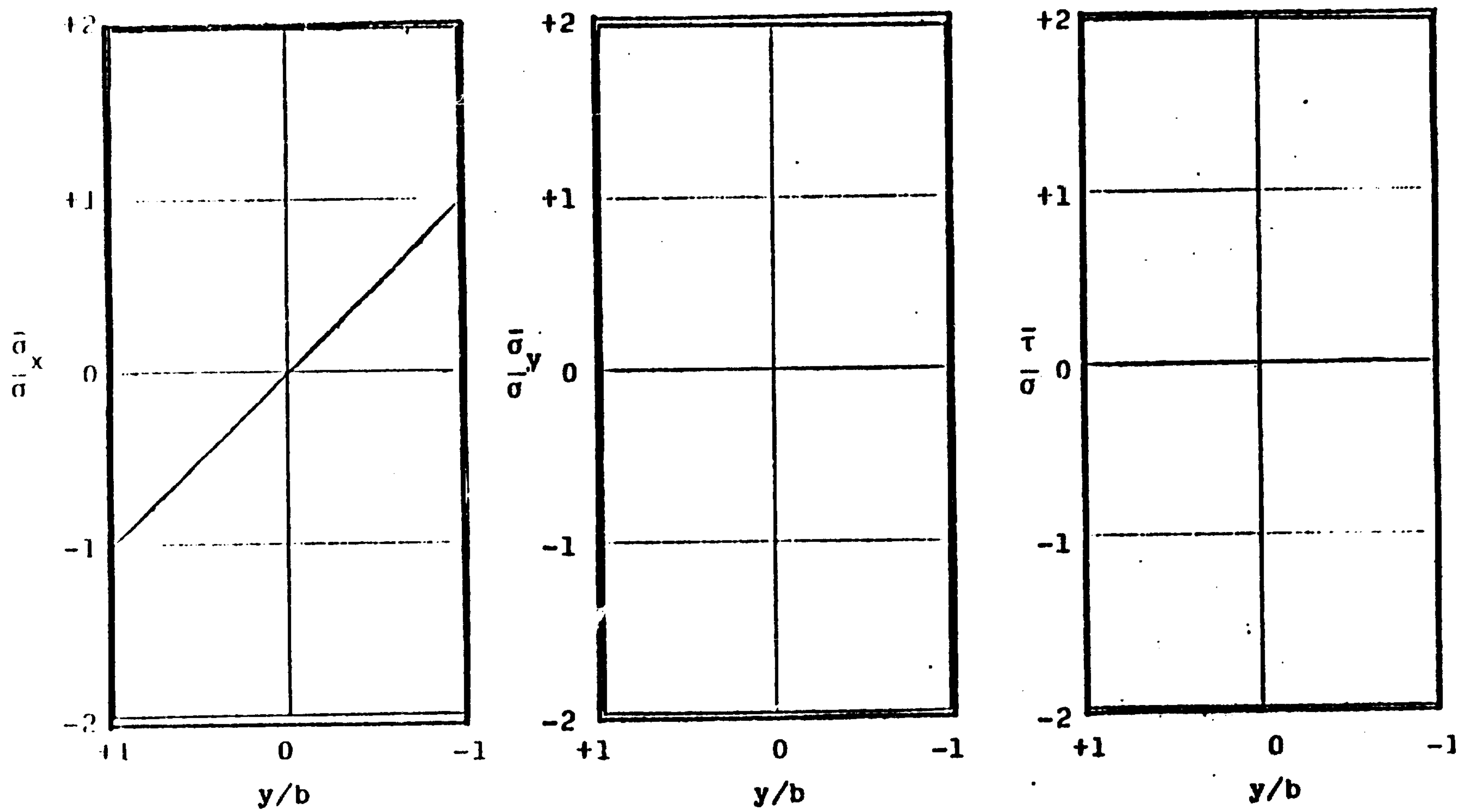

Figure 32 Bending, U-D laminate, ξ=6, x/L=1, N=3

TABLE 15. Eigenvalues for U-D laminate in pure bending

N	1	2	3
I-1	0.851	0.805	0.804
I-2		1.639	1.402
I-3			2.655
II-1	5.260	5.132	5.005
II-2		10.230	10.220
II-3			15.500

Chapter VI

SIGNIFICANCE

A general method of solving the two dimensional stress analysis problem for rectangular laminates subject to mixed boundary conditions has been presented. For compression sepcimens, the kinematic boundary conditions define the manner in which the load is introduced. The analysis presented herein assumes rigid body motion of the clamped edge; this assumption represents a "worst case" condition. In any actual experiment there will almost certainly be some deformation and/or even slippage in the fixture.

Quasi-isotropic specimens respond uniaxially at locations at least 3/4 of the specimen width away from the edge; for cross-ply, the uniaxial range in 1.50 width away from the edge. Since specimens tested in the IITRI fixture [1] have such short gage lengths, it may be concluded that a uniaxial response can not be developed in specimens* using this fixture.

---

* An exception is unidirectional laminates with small values of ν_{21}.

The constrained edge effect upon measured Young's modulus may be determined as follows. Let E_x and E^* denote, respectively, the actual modulus and experimentally determined modulus using strain gages at the location y along the center line. Thus

$$E^* = \frac{\sigma_c}{\varepsilon_x(o, y)} \quad . \qquad (33)$$

Combining (33) with Hooke's law (3) to eliminate the strain $\varepsilon_x(o, y)$, we obtain

$$\frac{E^*}{E_x} = \frac{\sigma_c}{\bar{\sigma}_x(o,y) - \nu_{xy}\bar{\sigma}_y(o,y)} \quad . \qquad (34)$$

The measured strain $\varepsilon_x(o,y)$ will normally contain contributions from in-plane and out of plane bending. Since the stresses are odd function of y, the bending effects may be eliminated by using several gages and averaging the results.

Equation 34 has been evaluated for quasi-isotropic and cross-ply[1] laminates at several locations y; the results are shown in Tables 16. and 17. Column (a) in each table indicates the predicted experimental error if gages were placed at y=0. Similarly, column (b) in each table

---

1 These results are based upon ν=0.336 for Q-I laminates, and ν=0.80075 and T_o=-1.176 for C-P laminates.

shows the predicted error if gages were placed at $y=\pm b/2$. Since, for each case, column (b) is closer to unity than column (a), placement of gages at $y=\pm b/2$ is a better location for strain gage placement. In fact, calculations at other values indicate $y=\pm b/2$ is the optimal location.

Column (c) in Tables 16 and 17 is based upon the assumption of three strain gages, two at the quarter points on one face and the third in the center of the opposite face. Clark and Lisagor [1] took extensive measurements of graphite/epoxy using strain gages at precisely these three points. Column (d) shows the experimental results based upon Clark and Lisagor's original data[1]. It will be observed that comparison of the theoretical results column (c) with the experimental result column (d) is exceptionally good for quasi-isotropic laminates. For cross-ply laminates, Table 17 shows a considerable discrepancy between predicted and actual error[2]. The experimental results confirm the greater sensitivity of modulus to aspect ratio for the cross-

---

1 Original stress-strain curves were available only for $\xi=0.25$, 0.50 and 1.0. For Q-I specimens, a "best-fit" straight line was constructed over the strain range $\varepsilon=0$ to $\varepsilon=0.006$. Average moduli for the three aspect ratios were 7.09x10 ksi, 6.71x10 ksi, 6.39x10 ksi. The actual modulus was assumed to be 6.59x10 ksi for purposes of completing the column.

2 Column (d) of Table 17 uses data as reported by Clark and Lisagor.

TABLE 16. Predicted experimental error of Young's modulus E for Q-I laminate

E^*/E_x				
	(a)	(b)	(c)	(d)
ξ	$\frac{E^*(0,0)}{E_x}$	$\frac{E^*(0,\frac{b}{2})}{E_x}$	$\frac{(a)+(b)}{2}$	E^*/E_x
0.25	1.091	1.063	1.077	1.083
0.50	1.026	1.007	1.017	1.018
1	0.962	0.986	0.974	0.970
3	0.999	1.000	0.999	—
6	1.000	1.000	1.000	—

TABLE 17. Predicted experimental error of Young's modulus E for C-P laminate

E^*/E_x				
	(a)	(b)	(c)	(d)
ξ	$\frac{E^*(0,0)}{E_x}$	$\frac{E^*(0,\frac{b}{2})}{E_x}$	$\frac{(a)+(b)}{2}$	E^*/E_x
0.25	2.38	2.32	2.35	1.13
0.50	1.93	1.43	1.64	1.01
1	0.82	1.19	0.97	0.97
3	1.02	1.01	1.02	1.00
6	1.00	1.00	1.00	1.00

plies, but not to the extent predicted. Presumably, the assumption of a rigid clamped edge is not appropriate for short gage length, high Poisson's ratio specimens in compression using the IITRI fixture.

A more plausible explanation is that the rather high stress levels near the constrained edge place the material well into the non-linear range of behavior. [Note the high stress levels at the edges in Figs 16,17]. Consequently, it is possible that the width of the specimen near the clamped edge expands non-linearly, thereby greatly diminishing the constrained edge effect.

For completeness, we point out that Clark and Lisagor [1] found that the modulus of unidirectional laminates was independent of ξ; this is consistent with the results of Chapter V.

Although an explanation of compressive failure of composites was not one of the objectives of this study, some preliminary results are obtainable directly from the stress analysis. Failure theories for single plies may be applied directly to the stress distribution within each individual lamina.

Delamination will occur when the interlaminar shear stresses τ_{zx} and τ_{zy} exceed the allowable loads for the epoxy. These shear stresses may be approximately obtained from the three-dimensional equilibrium equations, i.e.

$$t^{i}\cdot\left[\frac{\partial\sigma_x^{i}}{\partial x}+\frac{\partial\tau^{i}}{\partial y}\right]+\Delta\tau_{xz}^{i}=0,$$
$$t^{i}\cdot\left[\frac{\partial\tau^{i}}{\partial x}+\frac{\partial\sigma_y^{i}}{\partial y}\right]+\Delta\tau_{yz}^{i}=0, \qquad (35)$$

where the superscript i refers to the i-th lamina, $\Delta\tau$ refers to the difference in value of shear stress across the i-th lamina, and t^{i} the thickness of the i-th lamina. For small t^{i}, these shear stresses are very small, except where the in-plane stress exhibit large gradients.

Chapter VII

CONCLUDING REMARKS

Limitations of the Model

Insofar as the problem is analyzed as generalized plane stress, it will not provide an exact solution to the three-dimensional elasticity problem. In particular, the third equation of equilibrium (force-balance in the z-direction) will not be satisfied [15]. However, it is well known that the generalized plane stress solution is very close to the exact solution if the thickness of the laminate is small compared to the other two dimensions.

The linearity assumption Eqs. (3) is a somewhat more serious limitation of this model. Compression tests of uniaxial [0]s high-strength graphite/epoxy laminates indicate linear behavior between load and axial compressive strain all the way to fracture [1]. Since the load is carried predominantly by the graphite fiber, it may be inferred that graphite responds linearly to compressive rupture. On the other hand, a cross-ply $[\pm 45/\mp 45]_s$ stacking of the same laminae produces a non-linear behavior, particularly near failure. It is important to note that although the ultimate axial strain for cross-ply laminates exceeds the ultimate axial strain for unidirectional laminates by a factor of up to 3 [1], the maximum compressive fiber strain is considerably lower for the cross-ply than for the uniaxial layup. Indeed, these cross-ply laminates fail due to delamination and not fracture [1]. It may be inferred from the foregoing discussion, that the cross-ply laminate behaves non-linearly because the epoxy exhibits non-linear behavior. Such non-linear effects may also be observed from transverse strain measurements on unidirectional laminates. Ashton [16] reports varying values for Poisson's ratio during axial compression tests on high-strength graphite/epoxy composites. The inelastic behavior of composites was also investigated by Foye from the point view of micromechanics [17].

The model is very difficult to validate empirically, since it is impossible to know the exact kinematic boundary conditions at the clamped edges. It is evident that an edge constrained to respond rigidly is the severest case that might be encountered. The results obtained in this study should therefore be viewed as the "worst possible case".

Treatment of the constrained edge effect due to out of plane bending, while of technical interest, is not studied in this work. Such effects are expected to be small in comparison to in-plane bending because the Poisson ratio ν_{13} is generally much smaller than ν_{xy} and the thickness of most laminates is very small compared to their width. Moreover, a study of these effects would involve a considerably more complicated model.

Thus the developed model should only be considered a first approximation to an accurate description. It may be used by the experimentalist to corroborate only the inital portion of the stress-strain compressive data. At the other end of the data curve it may be used only to suggest, rather than provide definitive explanations, for different modes of failure.

BIBLIOGRAPHY

1. R.K. Clark and W.B. Lisagor, "Compression Testing of Graphite/Epoxy Composite Materials, "Presented ASTM Symposium on Testing and Design Allowables for Fibrous Composites, October, 1979, Dearbon. Also NASA Technical Memorandum 81796., Apr. 1980.

2. N.J. Pagano and J.C. Halpin, "Influence of End Constraint in the Testing of Anisotropic Bodies", Journal of Composite Materials, Vol. 2, 1968, pp. 18-31.

3. H.B. Phillips and C.L. Manti, "Two-Dimensional Study of Transverse Stresses in Axially Loaded Sections", Experimental Mechanics, Vol. 9, Mar. 1969, pp.137-139.

4. J.M. Whitney, G.C. Grimes and P.H. Francis, "Effect of End Attachment on the Strength of Fiber-Reinforced Composite ylinders", Experimental Mechanics, Vol. 13, May 1973, pp. 185-192.

5. M.S. Hess, "The End Effect for a Laminate Elastic-Strip, I. The General Solution, II. Differential Expansion Stresses, "Journal of Composite Materials Vol. 3, 1969, pp. 262-280, 631-641.

6. R.B. Pipes and N.J. Pagano, "Interlaminar Stresses Under Unifor, Axial Extension", Journal of Composite Materials, Vol. 4, October 1970, pp. 538-548.

7. S.D. Wang and F.W. Crossman, "Some New Results on Edge Effect in Symmetric Composite Laminates", Journal of Composite Materials, Vol. 11, Jan. 1977, pp. 92-106.

8. P.W. Hsu and C.T. Herakovich, "Edge Effects in Angle-Ply Composite Laminates", Journal of Composite Materials, Vol. 11, October 1977, pp. 422-428.

9. T.S. Wang and J.N. Dickson, "Interlaminar Stresses in Symmetric Composite Laminates". Journal of Composite Materials, Vol. 12, October 1978, pp. 390-402.

10. R.W. Jones, Mechanics of Composite Materials, Scripta

Book Washington, D.C., 1975.

11. S.P. Timoshenko and J.N. Goodier, Theory of Elasticity, McGraw-Hill, New York, 1970.

12. S.P. Timoshenko, Strength of Materials, Part, II, Van Norstrand, New York, 1956.

13. C.R. Wylie, Advanced Engineering Mathematics, 4-th Edition, McGraw-Hill, 1975.

14. B. Carnahan, Applied Numberical Methods, Wiley, New York, 1969.

15. I.S. Sokonikoff, Mathematical Theory of Elasticity, McGraw-Hill, 1956.

16. J.E. Ashton, J.C. Halpin and R.H. Petit, Primer on Composite Materials, Technomic Publishing Company, Stanford, Conn., 1969.

17. R.L. Foye, "Theoretical Post-Yielding Behavior of Composite Laminates. I, II-Inelastic Micromechanics", Journal of Composite Materials, Vol. 7, April 1973, pp. 178-193, 310-319.